Development of a digital X-ray-imaging system at the National Accelerator Centre.

Emari Lätti

A thesis submitted in partial fulfilment of the requirements for the degree of Master of Science in physics at the University of Stellenbosch

Supervisor: Dr. J. A. Stander

Co-supervisor: A. N. Schreuder

December 2000

I, the undersigned, hereby declare that the work contained in this thesis is indeed my own original work and that I have not previously in its entirety or in part submitted it at any university for a degree.

Signature:

Date:

Abstract

A digital portal X-ray imaging system was developed to replace the radiographic X-ray films currently used for patient position verification at the National Accelerator Centre (NAC) proton therapy facility. The main advantage of a digital system is the short time in which the image can be obtained. Other advantages include optimisation of the image display, effective archiving of the digital images, access from various locations through data networks, and lower operational costs. The digital system described in this thesis consists of a Gd_2O_2S:Tb scintillator screen for converting X-rays to visible light, a protected aluminum front silvered mirror to direct the light to a Charge Coupled Device (CCD) camera for capture and a personal computer for data acquisition, processing and display. Compared with other digital imaging systems, this is a simple, compact and affordable system.

The properties of the various components were investigated. The Rarex G-130 (Gd_2O_2S:Tb) scintillation screen was chosen for its good spatial resolution, high emission efficiency and good matching between the spectral emission wavelength peak and the quantum efficiency of the CCD camera. The spatial resolution measured for the system with a field of view (FOV) of 290 x 190 mm^2 is 1.3 lp/mm, which can be improved by increasing the CCD chip resolution or decreasing the field of view, since the CCD camera limits the spatial resolution. Intrinsic detector noise determines the lower limit of the dynamic range of the detector and is reduced by cooling the CCD camera. A dark current exposure is subtracted from the image to remove the bias signal and background signal level mainly caused by thermal noise. Photon noise, beam in-homogeneity and efficiency variations across the CCD chip are removed by a flat field correction. The digital images obtained with this system compare very well with the currently used radiographic film images and they are satisfactory for the purpose of patient position verification. Using the digital system it is possible to reduce the patient dose by 19 % and still obtain satisfactory image quality.

Opsomming

'n Digitale X-straalafbeeldingstelsel is ontwikkel om die radiografiese X-straalfilm wat tans gebruik word vir die kontrolering van die pasientposisionering voor die toediening van protonterapie by die Nasionale Versnellersentrum, te vervang. Die voordeel van die digitale sisteem is dat die beelde feitlik onmiddellik beskikbaar is. Verdere voordele sluit die optimisering van die vertoon van beeldkontras, effektiewe liassering, vinnige bereik deur datanetwerke en lae lopende kostes in. Die digitale sisteem beskryf in die tesis bestaan uit 'n gadolinium oksi-sulfied (Gd_2O_2S:Tb) sintillasieskerm wat X-strale omskakel na sigbare lig, 'n eerste-oppervlak aluminiumspieël wat die lig na 'n digitale kamera (CCD kamera) weerkaats en 'n persoonlike rekenaar vir dataverwerwing, verwerking en vertoon. Vergeleke met ander digitale stelsels is hierdie digitale beeldingstelsel eenvoudig, kompak en bekostigbaar.

Die eienskappe van die verskillende komponente van die stelsel is ondersoek. Die Rarex G-130 (Gd_2O_2S:Tb) sintillasieskerm is gekies vanweë goeie resolusie, hoë emissiedoeltreffendheid en die hoë omsettingsdoeltreffendheid van die digitale kamera by die spektrale emissiegolflengte van dié sintillasieskerm. Die ruimtelike oplosvermoë van die stelsel is bepaal met 'n veldgrootte van 290 x 190 mm^2 as 1.3 lynpare per millimeter. Die ruimtelike oplosvermoë kan verhoog word deur die kameraresolusie te verhoog of die veldgrootte te verklein, omdat die resolusie van die kamera tans die oplosvermoë van die stelsel beperk. Intrinsieke ruis van die detektor beperk die onderste grens van die dinamiese reikwydte van die detektor en kan verminder word deur die kamera te verkoel. 'n Donkerstroom-beeld word van die X-straalbeelde afgetrek om die voorspanningsein en die agtergrondsein, wat hoofsaaklik veroorsaak word deur termiese ruis, te verwyder. Ruis wat ontstaan as gevolg van fluktuasies in die aantal fotone, nie-homogeniteite in die bundel of variasie van die sensitiwiteit in die skerm word verwyder met behulp van 'n plat vlak beeld. Die digitale beelde verkry met die stelsel vergelyk goed met die beelde wat tans op film geneem word en die beeldkwalitiet is voldoende vir die kontrolering van die pasient-opstelling. Dit is moontlik om die pasiëntdosis met 19 % te verminder en steeds voldoende beeldkwaliteit te verkry.

Acknowledgements

I would like to thank the following people for their invaluable contributions towards this project:

Firstly, Nick Schreuder at the National Accelerator Centre for his continuous guidance and support throughout the project. Nick's combination of knowledge, expertise and enthusiasm is priceless and it is an honour to work with him.

Dr. Anton Stander, my academic supervisor at the Physics department, Stellenbosch University, for his advice and the interest he took in the project and his involvement during the past two years.

Alfons Kiefer at NAC for the construction of the box and help with all the experiments and measurements.

KlaasJan Renema, 'CCD team member', from the Netherlands for everything I have learnt from him and for a great friendship.

Dr. Katja Langen from NAC for all the help with the physics, presentations and posters. The radiographers at NAC (Shafeeqa, Shaheeda, Avril, Daphne) and Natalie, Medical Radiation Group NAC, for their encouragement and friendship.

I dedicate this thesis to the two greatest people on earth, my parents, Ivan and Mari Lätti.

Table of contents

List of Figures

List of Tables

Chapter 1

Motivation and outline of this thesis

1.1 Introduction

Patients have been treated with protons at the National Accelerator Centre since 1993 [Jon95]. The success of proton therapy relies on very accurate positioning of patients before treatment [Hou99]. After the patient has been positioned for treatment, the set-up position is verified using a portal X-ray image. These radiographic portal X-ray images are currently taken on X-ray film. The objective of this project was to develop a digital portal X-ray imaging system to replace the portal films.

1.2 Proton therapy patient positioning

Proton beams have a characteristic depth-dose curve with a high dose deposition peak near the end of the range, and a relatively low entrance dose (see Figure 1-1). This dose profile is referred to as the Bragg peak, named after William Bragg who first observed the peak for helium nuclei in air [Bo98a]. The Bragg peak makes it possible to confine the dose placement to the tumor and therefore deposit large doses very accurately. As a result, tumors located close to critical structures can be treated effectively while surrounding tissues are spared. It is therefore important that the patient is positioned accurately in the proton beam.

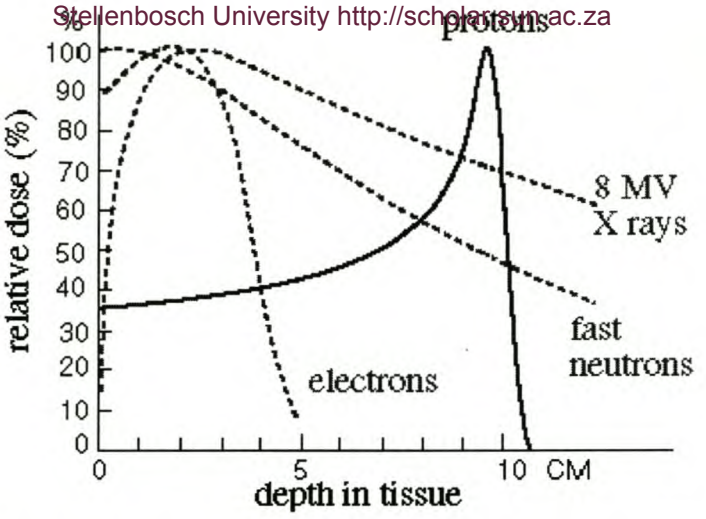

Figure 1-1: Depth dose curves of protons, X-rays, fast neutrons and electrons.

Patients receiving proton therapy at the National Accelerator Centre are positioned using a stereophotogrammetric (SPG) patient positioning system [Hou99]. This system makes use of fiducial markers (1 mm steel balls) and reflective disks placed in a custom made mask (see Figure 1-2). The mask fits tightly over the patient's head and is fixed to the treatment chair to keep the patient in the correct position for the duration of the treatment. Three-dimensional co-ordinates for each of the fiducial markers are obtained from a CT scan taken during the treatment preparation (treatment planning phase). The CT scan is also used to determine the position of the markers relative to a reference point in the treatment volume in the same co-ordinate system. The reflective disks are carefully fixed to the mask in such a way that the centre of the disk coincides with the fiducial marker in the mask. Three out of eight CCD cameras in the treatment room (see Figure 1-3) are used to determine the position of the reflective disks on the mask. The reflections from these markers are used to position the mask, and hence the patient, using the SPG system. The co-ordinates of the markers are sent to the SPG computer to determine the position of the patient relative to the proton beam, compared to the planned position. The necessary adjustments to the position are then sent to a second computer that controls the chair to move the patient into the correct position.

Figure 1-2: Proton therapy treatment room.

Since the markers are used for positioning, it is necessary to verify that the position of the mask relative to the anatomy agrees with the position during the CT scan from which the treatment plan was constructed. For this reason the patient position is verified for each treatment field by comparing a radiographic portal X-ray image of the patient to the digitally reconstructed radiograph (DRR), obtained from the treatment planning system. The DRR is constructed from a CT scan of the patient wearing the mask and contains the position of the fiducial markers relative to the treatment volume. The X-ray tube is placed upstream of the collimator in the beam line to take a radiographic image of the patient on X-ray film placed behind the patient as illustrated in Figure 1-3.

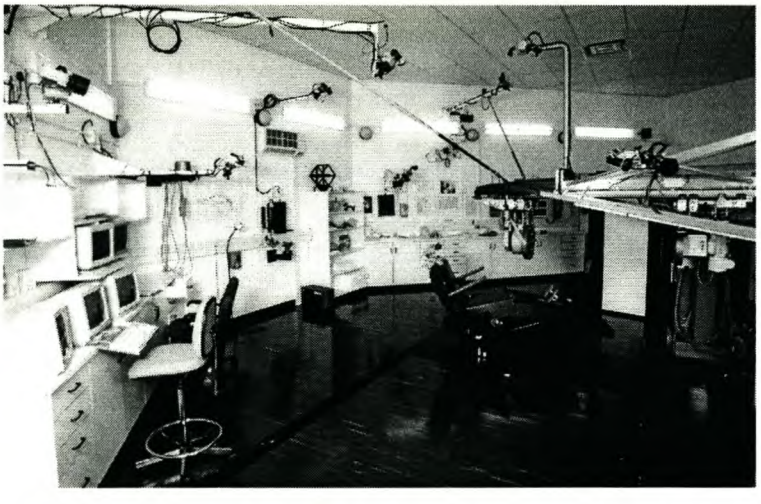

Figure 1-3: Position of the collimator, patient mask and X-ray film.

The radiographic X-ray image shows the positions of the steel balls (markers) relative to the anatomy. The X-ray image is compared with the DRR to confirm whether the patient may be treated. The X-ray image and DRR for the same treatment field are shown in Figures 1-4 and 1-5 below.

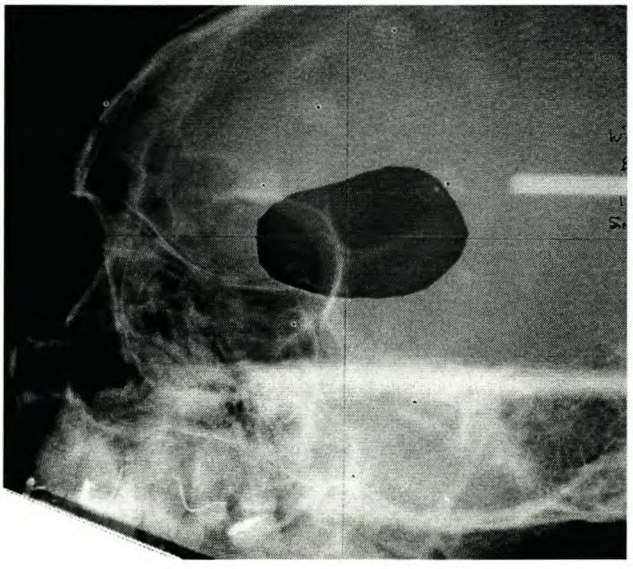

Figure 1-4: X-ray image of the patient indicating the steel balls on the mask and the outline of the collimator with respect to the anatomy.

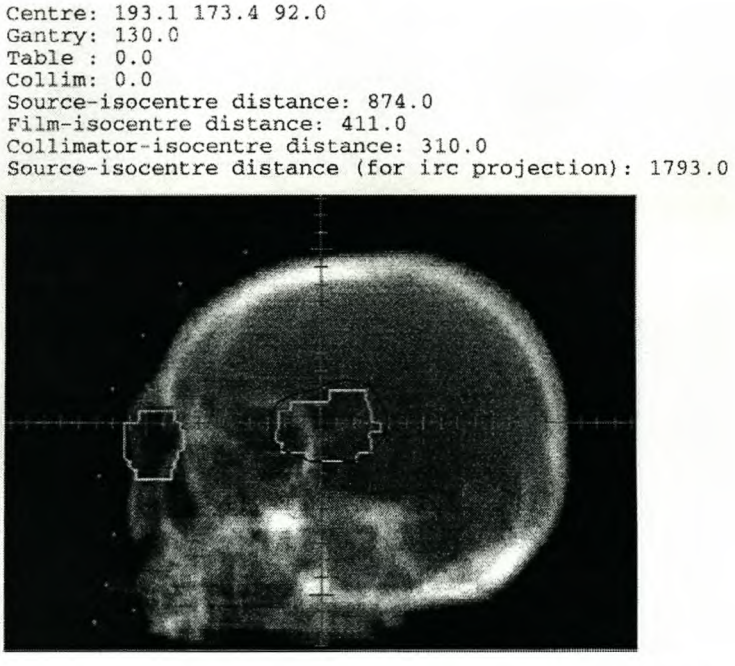

Figure 1-5: Digitally reconstructed radiograph (DRR) obtained from the treatment planning system for the same treatment field as in Figure 1-4.

1.3 Motivation for this project

A digital imaging system has many advantages over portal films. While film takes a long time to develop, a digital imaging system offers real time imaging. A considerable amount of time is lost during the development of the portal X-ray films, which takes about 90 seconds, and walking between the treatment room and the darkroom. On the contrary, digital images are available within seconds after the X-ray image is taken. Another advantage is that the images are available in digital form, which means that the comparison with the DRR can be done using computer software. This again saves time and is also a more accurate method of comparison.

Furthermore the digital imaging system allows for variable contrast display whilst the contrast on film is fixed [Alt96]. The possibility of controlling display contrast eliminates the need for repeating an X-ray exposure in the case of over-exposure or non-optimal blackening of film. However, the spatial resolution of digital systems is lower than portal film resolution, due to light scatter between the screen and the CCD camera, which is not present in a screen-film system, and the limited resolution of the CCD camera.

The digital imaging system described in this thesis has a simple design and also has low operational costs compared to the expensive chemicals and X-ray film of the current system.

1.4 The scope of the project

This thesis presents an investigation of a scintillation screen and CCD (Charge Coupled Device) camera digital imaging system. There are various alternative digital imaging systems available, for instance flat panel detectors (amorphous selenium), storage phosphor screens, CMOS (Complementary Metal Oxide Semiconductor) detectors, fibre optically coupled scintillators, systems using image intensifier or photon multiplier tubes and many more [Har88], [Boy92], [Fah95]. In amorphous selenium detectors, X-ray photons are directly converted to an electronic signal. The optical component is therefore absent and a higher spatial resolution can therefore be obtained using an amorphous selenium flat panel detector, [Nei94]. A fibre optically coupled imaging system makes use of phosphor screen to convert X-rays to visible light. The phosphor screen is coupled to a fibre optic light channelling device, (fibber optic tapers or light guides) that transports the light to the CCD detector, [Ham99]. These digital imaging systems are

considerably more expensive than scintillation screen – CCD systems. CMOS detectors are similar to CCDs and are also used as camera sensors. They differ from CCD detectors in that they do not store or transfer electric charge; signals are read out immediately after light detection. Furthermore, each detector element is capable of performing basic electronic operations such as analog to digital conversion and arithmetic logic operations. There is also no pixel saturation, as found with CCD detectors. The current drawback of these detectors is the readout-noise contribution, producing lower image quality, but this will be improved as the CMOS technology improves [Ind99].

1.5 Outline of the thesis

The purpose of this thesis is to describe the physical principles involved in digital X-ray imaging and to serve as a guideline for the design and testing of similar imaging systems.

The physical principles and application of X-ray imaging, namely X-ray production, interactions and detection are investigated in Chapter 2.

Chapter 3 describes the digital imaging system set-up and the experiments performed to evaluate the performance of the system and its individual components. The system is evaluated in terms of the light yield, spatial resolution, image quality and also the dose delivered per exposure. Methods to focus the camera, to improve image quality and to measure the spatial resolution are presented.

In Chapter 4 the results of experiments for measuring the performance of the components are discussed. Recommendations for the selection of components and adjustments to the system to improve the image quality are discussed and presented in Chapter 5.

Chapter 2

Theoretical background

2.1 Introduction

This chapter contains a summary of the physical principles involved in X-ray image formation. The production of X-ray photons and how their interactions influence image quality and radiation dose to the patient are considered. Image acquisition based on the conversion of X-rays to light, light collection and detection is described. Methods for evaluating the performance of the imaging system in terms of various aspects of image quality as well as dose measurement are presented.

An imaging system receives and captures a two-dimensional input signal to produce an output signal or image. If the output is a radiographic image, the input signal is a representation of the attenuation of X-ray photons in a patient. The amount of attenuation in the patient depends on the elemental composition as well as the physical state of the tissue material and is higher for elements with high atomic number and high-density materials. The difference in attenuation for different paths produces a difference in X-ray intensity that supplies the required contrast to form the radiographic image. It is important to know how the X-ray photons interact in the patient to produce a high contrast image and how this image can be recorded.

The electromagnetic spectrum may be divided into non-ionising and ionising parts. If the energy of electromagnetic radiation is sufficient to remove orbital electrons during an interaction with an atom in a medium, it is referred to as ionising radiation. The energy of non-ionising radiation (wavelengths 100 nm and longer) is too low to ionise the atoms in a material. X-radiation forms part of the ionising spectrum and lies between approximately 1 to 10^{-3} nm in the wavelength region [Mer79]. Gamma rays have higher energy and form part of the electromagnetic spectrum with shorter wavelengths. The distinction between X-rays and gamma rays is made in terms of the origin of the radiation, since the low energy gamma ray region and high-energy X-ray region overlap. Gamma rays originate from interactions in the nucleus and X-rays from interactions outside the nucleus.

Electromagnetic radiation may also be described as propagating particles or packets of energy, rather than waves. Each 'packet' is called a photon and carries energy equal to

$$E = h\nu \tag{2-1}$$

where h is Planck's constant (6.62×10^{-34} J s). Using $c = \lambda\nu$, with $c = 2.998 \times 10^{8}$ m s^{-1}, the photon energy is easily obtained from its wavelength by

$$E = h\frac{c}{\lambda} = \frac{1.24}{\lambda} \text{ [MeV]} \tag{2-2}$$

2.2 Production of X-rays

Electrons are accelerated inside a vacuum-sealed X-ray tube between a negative electrode or cathode (filament) and a positive electrode or anode (target), placed at opposite ends inside the tube. X-rays are produced when the accelerated electrons collide and interact with the anode.

Electrons are produced from thermal emission by applying a low voltage (about 10 V, supplying 3.0 A to 5.5 A) circuit across the filament at the cathode end of the X-ray tube [Cur90]. The temperature of the filament should be at least 2200°C to emit a sufficient amount of electrons for the production of X-rays. Tungsten with its high melting point of 3370°C and high atomic number is therefore often used as filament material [Mer79].

The free electrons are focussed to the target by a negatively charged nickel focussing cup placed around the filament. The electron beam is then collimated to a well-defined area on the anode called the focal spot. X-ray tubes often have two filaments of different sizes to obtain different focal spot sizes. The focal spot size influences the spatial resolution of an image because a finite size focal spot is used instead of a 'point source'. The focal spot causes a shadow or penumbra around the image, which reduces image sharpness (see Figure 2-18 in section 2.7.5, spatial resolution). However, more heat is produced per unit area of a small focal spot, which limits the filament current and exposure times. The focal spot should therefore be large enough to accommodate the amount of heat produced, since increasing the focal spot size increases the amount of heat endurance of the anode. The penumbra formed by the focal spot is only one of many factors adding to the reduction in image sharpness and it can be kept small by using as small a focal spot as possible [Mer79].

X-rays are produced when accelerated electrons interact with the atoms in the target. These electron interactions are described below in sections 2.2.1-2.2.3. Tungsten is used as target material because of its high atomic number and therefore high interaction probability. With repeated exposures, the heat build-up becomes very high and can cause permanent damage to the target. During a single exposure with a tube voltage of 100 kV, less than 1 % of the electron energy is converted to X-rays and 99 % contributes to the production of heat. The tube voltage, anode size and exposure time set an upper limit for the tube current necessary to avoid possible damage to the target. The tungsten target is imbedded in a copper housing through which the heat can be dissipated, since copper is a better conductor than tungsten. Another way to deal with the build-up of heat is to replace the stationary anode by a rotating anode. By rotating the anode, the effective area of the anode is enlarged so that the heat produced during an exposure is spread over the whole area of the anode.

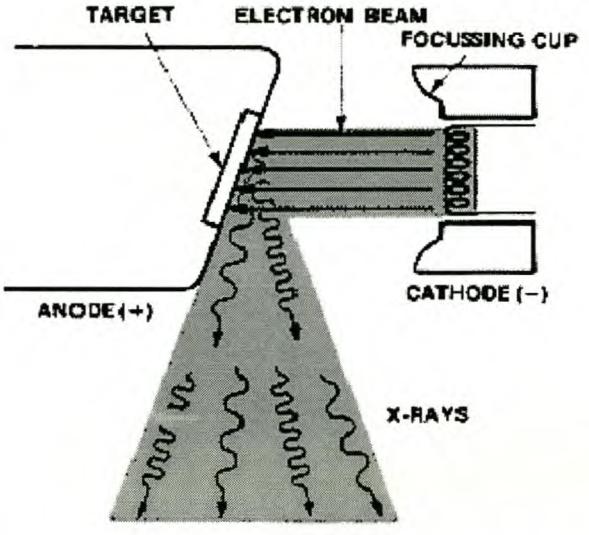

Figure 2-1: Production of X-rays. From The Fundamentals of Radiography, Rochester, 1980.

Electrons are accelerated to the anode or target by connecting a high voltage circuit to the anode and cathode. If there are no interactions with air molecules on their way, the electron will hit the target with an energy determined by the voltage across the electrodes (tube voltage), given by $E = q\,V$, where q is the charge of an electron and V the tube voltage. The tube voltage is pulsed and its magnitude varies between zero and its maximum or peak value. The voltage is expressed as kilovolt peak (kVp) which refers to the peak voltage across the X-ray tube. An electron acquires energy equal to eV, with V being the instantaneous potential across the tube.

The vacuum inside the tube is kept very high, to minimise collisions with air molecules. Collisions with air molecules firstly cause unwanted loss of kinetic energy of the electrons and secondly contribute to the production of secondary electrons by ionisation of the gas. These secondary electrons will also be accelerated towards the target and this will result in an uncontrollable amount of lower energy electrons arriving at the target. This will add to the low energy part of the X-ray spectrum.

Interaction between an electron and other charged particles through their Coulomb field is described by charged-particle Coulomb-force interactions. The type of interaction depends on the impact parameter of the incident electron, as described in the next three sections (2.2.1-3). The impact parameter gives a measure of the directness of the collision. The impact parameter is defined as the shortest perpendicular distance between the incident trajectory of the electron and the centre of the atom it collides with [Hal93].

2.2.1 Electron interactions with a target atom as a whole

If the impact parameter is very large compared to the size of the atom, the incident electron interacts with the atom as a whole. The varying electric field of the incident electron interacts with the atom, which is ionised or left in an excited state. After excitation, the atom loses its excess energy mostly through the emission of low energy radiation. In many cases the atom is left in a vibrational state, which results in the production of heat. Interactions with the whole atom contribute primarily to the total heat production inside the X-ray tube.

2.2.2 Electron-electron interactions

When an incident electron passes close to an atom with the impact parameter comparable to the size of the atom, the electron will most likely interact with a single electron inside the atom. If the energy of the incident electron is more than the binding energy of the electron, the bound electron will receive enough energy to escape. The secondary electron is ejected from the atom with sufficient kinetic energy to undergo Coulomb force interactions with other atoms. This electron is referred to as a delta (δ) ray and contributes to the production of X-rays in the same way as the incident electron but displaced from the original position of interaction.

After the emission of an electron the atom is left in an excited state for a short period of time, typically not longer than a nanosecond for solid materials, and an electron from a higher energy level fills the vacant position. An X-ray photon with energy equal to the difference in the energies of the two levels is released. This radiation is characteristic of the specific element and the specific orbital shells, and is referred to as characteristic X-rays.

Electrons in the K shell (innermost shell) are the closest to the nucleus and have the highest binding energies – about 70 keV for tungsten (Figure 2-2). If an electron from a higher shell fills the K shell, the resulting X-radiation is referred to as K-characteristic X-rays. If the electron decays from the L shell, the resulting X-photon carries energy equal to the energy difference between the K and L shells and is called a K_α X-ray. An electron from the M to the K shell will radiate a K_β X-ray and from M to L, an L_α X-ray. The maximum X-ray energy corresponds to a transition from a free electron to the K shell. The characteristic X-ray energy is higher for materials with high atomic number, since the binding energy of K shell electrons increases with atomic number [Kno89]. The energy spectrum formed by the characteristic X-rays is called the characteristic X-ray spectrum.

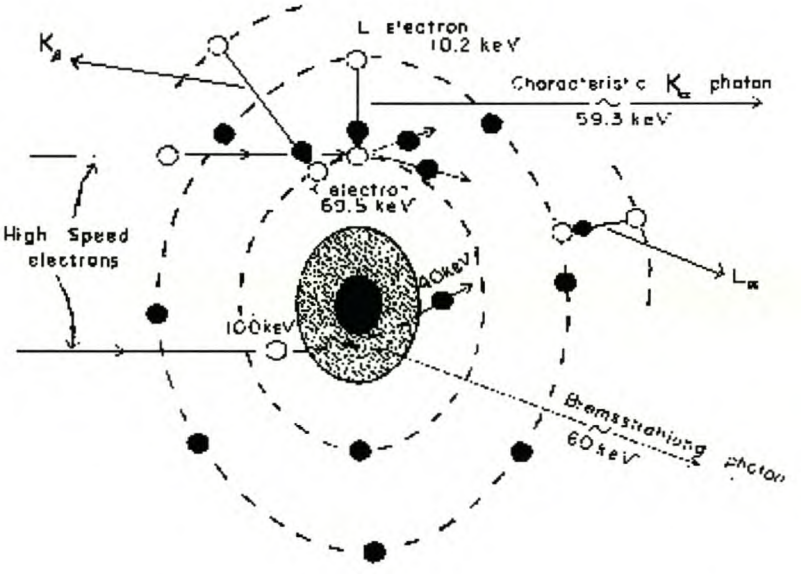

Figure 2-2: Illustration of typical electron interactions with atoms in a tungsten target involved in the production of X-rays (taken from [Spr93]).

The probability for the emission of a characteristic K shell X-ray photon increases rapidly for materials with atomic number greater than 10 and is close to unity for high atomic numbers

[Att86]. The emission probability for characteristic X-ray photons from the L shell is considerably lower and increases to approximately half of that for the K shell at high atomic number materials. The emission of characteristic X-ray photons from the M shell or higher has a very small probability [Att86].

The contribution of the characteristic spectrum to the total X-ray spectrum depends on the anode material, the tube voltage and the amount of filtering. The energy of the L series is normally too low to penetrate through the glass window of the tube and only the K series has a significant contribution to the spectrum. The glass window is especially thin to minimise X-ray absorption [Mer79]. For tube voltages between 80 kVp and 150 kVp the characteristic spectrum contribution is about 10 % of the total dose given to the patient [Mer79].

An excited atom can also lose its excess energy through the emission of one or more Auger electrons. If an inner shell vacancy is created by a preceding interaction such as photoelectric absorption, the excitation energy can be used to eject another electron, called an Auger electron, from an outer shell of the atom. During this process electrons in the atom rearrange themselves to fill an inner shell vacancy and an electron in an outer shell is ejected to release the excess energy. The energy of the Auger electron is equal to the difference between the binding energy of the initial shell and the binding energy of the shell from which the Auger electron is released. The vacancies in the outer shells are filled by electrons in the conduction band [Att86]. The production of Auger electrons is very low in materials with high atomic number because of the high electron binding energies and the contribution of Auger electrons to the production of X-rays is insignificant [Kno89].

2.2.3 Bremsstrahlung

If the impact parameter is much smaller than the radius of the atom, the electron will be attracted by the Coulomb field of the nucleus and be deflected from its path. The deflection causes a change in the velocity of the incident electron, which results in the emission of an X-photon (Bremsstrahlung) to conserve the momentum. An electron loses a part or all of its energy per interaction, depending on the degree of deflection, which means that the energy spectrum of radiation produced by Bremsstrahlung is continuous, with photon energies ranging up to the incident electron energy. The Bremsstrahlung energy spectrum is therefore also called the continuous X-ray energy spectrum.

The continuous energy spectrum has a distinctive cut-off wavelength. The minimum wavelength (maximum energy) corresponds to the interaction in which an incident electron with maximum energy (equal to the maximum tube voltage) loses all its energy in a single encounter. This wavelength is independent of the target material and is given by

$$\lambda_{\min} = \frac{hc}{eV} \quad . \tag{2-3}$$

The differential energy loss per path length for electrons through Bremsstrahlung is proportional to the electron energy and the atomic number of the target material as shown by equation 2-4 [Kno98].

$$\frac{\mathrm{d}E}{\mathrm{d}x} \propto EZ(Z+1) \tag{2-4}$$

When electrons interact with atoms inside the target, they can be deflected at large angles and even be scattered backwards. Backscattering mainly occurs for low electron energies and high atomic number targets. These electrons will then interact in one of the above mentioned ways and contribute to the low energy part of the Bremsstrahlung energy spectrum.

2.2.4 X-ray energy spectrum

The X-ray spectrum consists of the continuous Bremsstrahlung energy spectrum and the characteristic X-ray energy spectrum. The X-ray energy spectrum depends on the energy of the incident electrons as determined by magnitude and waveform of the applied voltage and also on the anode material. Another important factor is the amount and type of filtration placed in the beam (see Figure 2-3 below).

2.2.5 Exposure settings: kVp and mAs

The X-ray intensity or number of X-rays produced depends on the atomic number of the target material, the tube voltage (kVp), filament current (mA) and exposure time (s). The interaction probability of electrons in the target is higher for materials with high atomic number.

Furthermore the number of X-rays produced is proportional to the square of the tube voltage: Intensity $\propto Z\,(\mathrm{kVp})^2$ mAs [Mer79] and also depends on the applied voltage waveform. The number of X-rays produced with a constant applied voltage will be higher than for an alternating voltage of the same magnitude. A higher filament current will produce more electrons and therefore give rise to more interactions in the target to form X-rays. The number of X-ray photons also depends on the exposure time – more X-rays will be formed for more electrons incident on the anode. The product of the filament current and the exposure time (mAs) therefore is a measure of the number of photons that are produced.

2.2.6 Filtration

Without filtration, most of the low energy X-rays will be absorbed in the first few centimetres of the patient. This part does not contribute to the image but only increases the dose to the patient. The low energy component of the X-ray spectrum is therefore removed from the beam by filtration.

The X-ray beam is firstly filtered by the components in the tube, for example the glass window through which the beam passes. This filtration is called inherent filtration. Additional filtration is carefully selected to remove the low energy photons in order to increase the ratio of useful X-ray photons for imaging to the photons that only contribute to dose in a patient by removing the low-energy radiation in the beam. This produces an X-ray beam with higher average energy and therefore higher penetration; also known as beam hardening. Increasing the average energy of the X-ray beam is often referred to as increasing the quality of the beam. The quality of the beam refers to the penetrating ability, which depends on the energy of the individual photons. The amount of filtering and the tube voltage therefore determine beam quality.

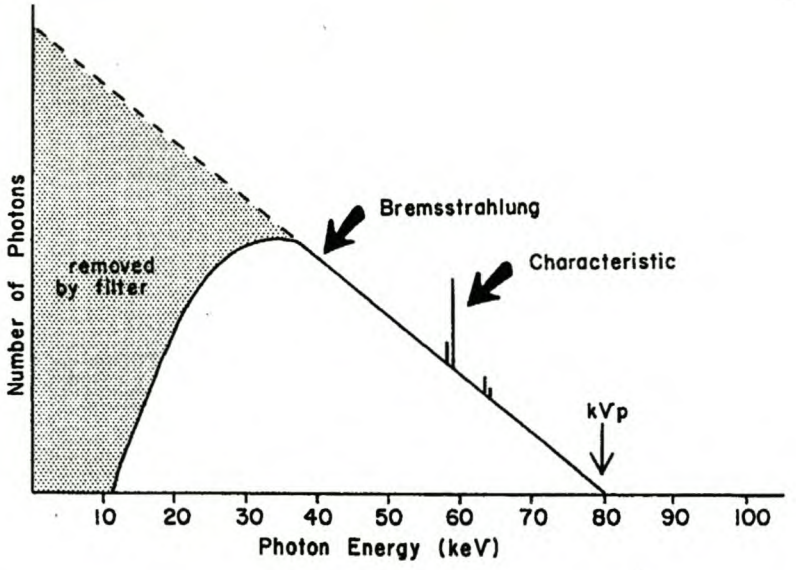

Figure 2-3: X-ray energy spectrum – continuous and characteristic spectra with the removal of low energy X-rays by filtration [Spr93].

The X-ray beam energy used in radiography is chosen carefully for every application. The diagnostic X-ray energy range is between 20 and 150 keV. For energies lower than about 20 keV, the dose to the patient is very high, and for X-rays with energy higher than 150 keV, the contrast is very low and values between these two extremes are normally used.

2.3 X-ray interactions with matter

2.3.1 Attenuation

Knowledge of how X-ray photons interact inside the patient, specifically how absorption and scattering of the X-ray beam in different parts of the patient will effect the image, can be used to optimise the image contrast using the lowest possible dose. Scattered radiation decreases image sharpness and should be kept as low as possible. High absorption leads to the production of high contrast images, but also increases the dose absorbed in the patient.

As the X-ray beam passes through the patient, the beam intensity decreases because of the attenuation of photons. The number of X-ray photons in an X-ray beam that will be attenuated in a material depends on the number of photons incident on the material, the interaction probability and the thickness of the material through which the beam moves.

Charged particles are directly ionising particles and lose their energy by interacting with almost every electron or nucleus they pass. Uncharged particles such as X-ray photons and neutrons deposit their energy indirectly through interactions producing secondary charged particles. Unlike charged particles, uncharged particles do not necessarily interact when they move through a medium. X-ray photon interactions occur randomly and there exists a probability for a specific interaction, which depends on the nature of the interaction. The fraction of the original photon beam that is removed per unit path length in the material is always constant for a given material [Mer79]. This relation is given mathematically by

$$\frac{dN}{dx} = -\mu N \tag{2-5}$$

where N is the number of photons, x the thickness of the material and μ is called the linear attenuation coefficient [Kno89]. By integrating this expression over the whole thickness L of a medium $x \in [0,L]$ and $N \in [N_0,N_L]$ the number of photons found in each corresponding position in the medium, yields the exponential relation

$$\frac{N_L}{N_0} = e^{-\mu x} \tag{2-6}$$

where L is the thickness of the medium, N_L and N_0 the transmitted and incident number of X-ray photons respectively. The X-ray beam is therefore attenuated exponentially with increasing depth in the medium and the decrease in the number of photons is given by equation 2-6. The linear attenuation coefficient μ is the fractional reduction of the number of X-rays per unit thickness.

The linear attenuation coefficient can also be interpreted as a representation of the probability for a certain interaction to occur per unit path length. The linear attenuation coefficient depends on the density of the material since more photons will be attenuated per unit mass in materials with higher physical density. The mass attenuation coefficient, given by the linear attenuation coefficient divided by the density of the material, is therefore normally used as a measure of the attenuation.

The important interactions of X-ray photons in the diagnostic energy range are elastic scattering, photoelectric absorption and Compton scattering.

2.3.2 Elastic scattering

Elastic scattering refers to interaction of an X-ray photon without a change in its energy (wavelength). There are two types of elastic scattering, namely Thomson and Rayleigh scattering. In Thomson scattering, the incident X-ray photon interacts with a single, bound electron in an atomic shell. The X-ray photon causes the electron to oscillate and the electron then emits an X-ray photon of the same energy as the initial photon. Rayleigh scattering, also called coherent scattering, describes the interaction of a photon with all the electrons of an atom. In this case the passing photon sets all the electrons in the atom into a vibrational state and the electrons vibrate at the same frequency as the incident photon. The atom returns to its ground state when the electrons again emit an X-ray photon of the same wavelength as the initial X-ray photon wavelength. The mass attenuation coefficient for Rayleigh scattering interaction is proportional to the square of the atomic number of the material and indirectly proportional to the X-ray energy: $\frac{\sigma}{\rho} \propto \frac{Z^2}{h\nu}$ and is therefore higher for lower energy X-rays interacting with a material with high atomic number [Att86]. The contribution of elastic scattering to the total attenuation of the X-ray beam is only a few percent and is not considered to play a role in the formation of X-ray images.

The most important interactions of X-rays for diagnostic imaging are photoelectric absorption and Compton scattering.

2.3.3 Photoelectric absorption

In photoelectric absorption an X-ray photon transfers all its energy to a bound atomic electron and disappears. This interaction occurs with electrons in inner atomic shells since it is not possible for a photon to transfer all of its energy to a loosely bound outer shell electron. If the photon energy is higher than the binding energy of the orbital electron, the electron uses the energy to escape from its shell and carries the remainder of the energy as kinetic energy. The kinetic energy T of the released electron is therefore given by

$$T = h\nu - E_B, \tag{2-7}$$

where $h\nu$ is the energy of the incident photon and E_B the binding energy of the electron in the particular shell [Kno89]. The photoelectron loses its energy through interactions with atoms in

the medium, as described in sections 2.2.1 to 2.2.3 (electron interactions). The release of the electron produces a vacancy that may be filled by a free electron, which again results in the emission of characteristic X-rays or from the rearrangement of electrons inside the atom (Auger effect, section 2.2.2).

The derivation of the interaction probability for the photoelectric absorption is complicated by the fact that the electron is bound to an atom and the interaction probability is described in terms of empirical results. The photoelectric mass attenuation coefficient is given by

$$\frac{\tau}{\rho} \propto \left(\frac{Z}{h\nu}\right)^3 (\mathrm{cm}^2/\mathrm{g}), \tag{2-8}$$

where Z is the atomic number of the material, $h\nu$ the photon energy and τ the linear attenuation coefficient for photoelectric absorption [Att86]. Equation 2-8 indicates that the mass attenuation coefficient for the photoelectric effect is proportional to the third power of the atomic number and decreases with increasing energy as also illustrated in Figure 2-4. The discontinuities in the graph of the mass attenuation coefficient where the mass attenuation coefficient rapidly increases are known as absorption edges. These edges appear when the X-ray photon energy is equal to the binding energy of an inner electron shell. The mass attenuation coefficient decreases with increasing photon energy until the photon energy is equal to the binding energy of an inner shell electron. Photons with energy equal to the binding energy of a specific shell will predominantly interact with electrons in this shell, resulting in a sharp increase in the mass attenuation coefficient at this energy.

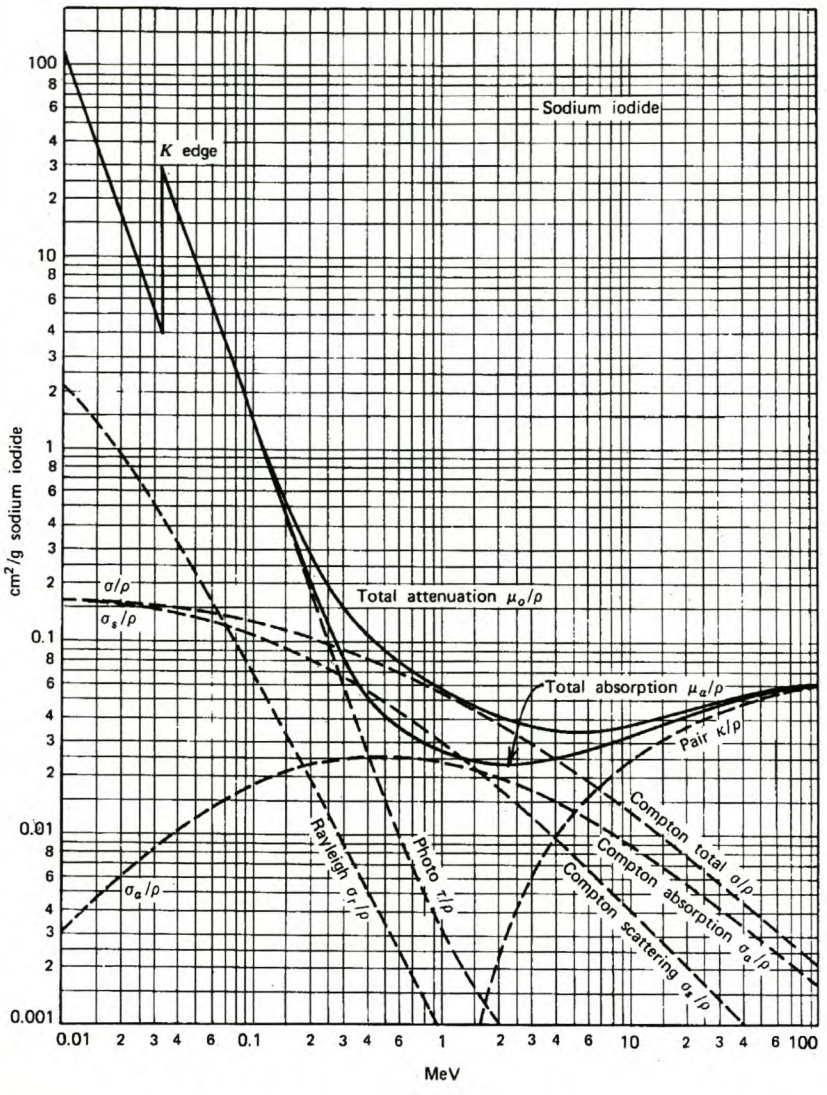

Figure 2-4: Graph illustrating the energy dependence of X-ray and gamma interaction processes in sodium iodide [Kno89].

2.3.4 Compton scattering

Compton scattering describes the process during which an X-ray photon interacts with an electron in an outer shell with binding energy much less than the photon energy. The photon transfers a part of its energy to the electron and moves off with lower energy and changed direction. The electron proceeds from its original position with kinetic energy equal to the energy lost by the photon.

The mass attenuation coefficient for Compton scattering is independent of the atomic number of the material [Att86]. Compton scattering is the dominant interaction at high photon energies (see Figure 2-5).

Compton scattering gives the biggest contribution to scatter in a patient and reduces image contrast compared to the photoelectric effect.

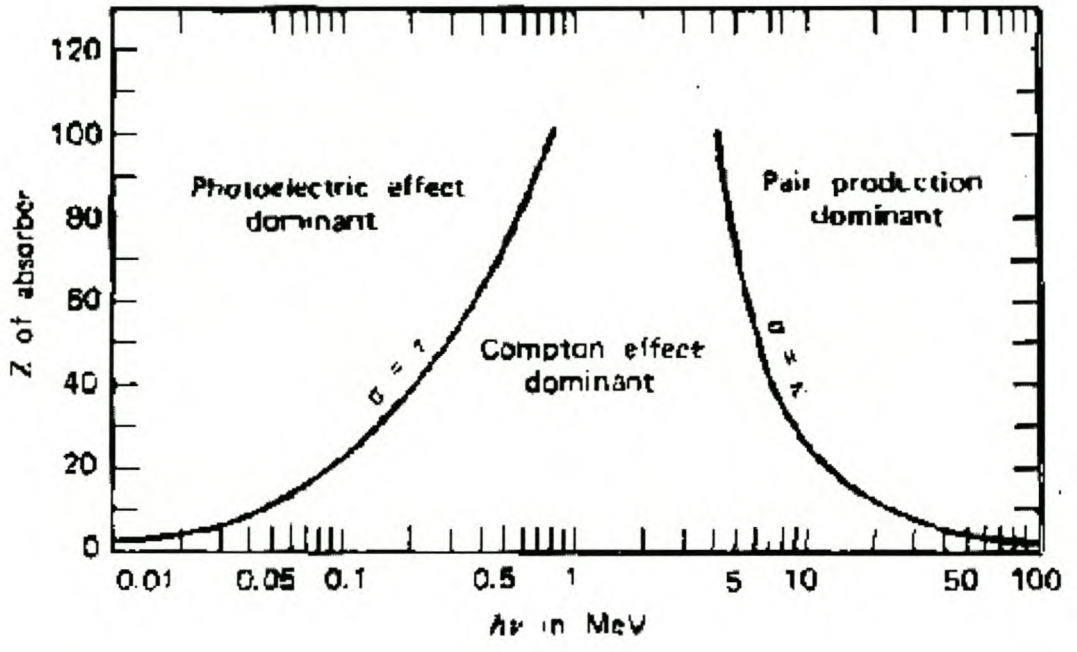

Figure 2-5: The relative probability of interaction for the processes photoelectric absorption, Compton scattering and pair production, taken from [Kno89]. Photoelectric absorption is predominant at low X-ray energies and Compton scattering occurs more at higher photon energies.

Since the linear attenuation coefficient depends on the tissue density (see section 2.3.1), materials with high densities cause more attenuation of the X-ray beam than low-density materials. This is especially true for low photon energies where the probability for photoelectric absorption is high (see Figure 2-4). For example, bone has a higher density than soft tissue. At low X-ray energies, bone matter absorbs much more of the beam than soft tissue and because the difference in transmitted beam intensity between bone and soft tissue is high, the contrast in the image will also be high. As the X-ray energy is increased, the difference in amount of attenuation between bone and soft tissue becomes smaller because of the increased penetrating power through bone.

The difference in attenuation between bone and soft tissue is therefore only prominent at low energies.

The photoelectric effect is the dominant interaction at low energies (X-rays) whilst Compton scattering is the dominant at higher photon energies, as illustrated in Figure 2-5.

2.4 Scintillation theory

Materials that emit light when excited are referred to as luminescent materials or scintillators. Scintillators can be divided into fluorescent, phosphorescent, thermoluminescent (stimulated by heat) and photoluminescent (stimulated by laser) materials according to the stimulation mechanism involved. Fluorescent materials radiate light instantaneously (time lag up to $\sim 10^{-8}$ s) after excitation and this is also called prompt emission. Phosphorescent materials emit light with a measurable time delay after excitation. We will focus on fluorescent materials, which are used in radiology (stimulated by X-ray photons) where time delay after excitation is undesirable. Scintillators may be organic or inorganic materials and the interactions of X-rays in the materials depend on the type of scintillation material.

2.4.1 Inorganic scintillators

Inorganic scintillators are available as powders or crystal structures (examples: Gd_2O_2S:Tb is available as a powder and CsI:Tl as a crystalline structure and also in powder form) [Mci99], [Ham99].

X-ray photon interactions with atoms in an inorganic scintillator material depend on the crystal lattice structure of the scintillator [Ham99]. The crystal lattice determines all the properties of the material and on atomic scale it determines the energy states of electrons in atoms. The energy level structure of a crystal lattice is composed of discrete energy bands separated by a forbidden region. Electrons inside the atoms that form the crystal structure are confined to these bands, which means that electrons will only have energies in the region determined by the limits of the allowed energy bands. Electrons in the valence band are bound at lattice sites, whilst electrons in the conduction band have enough energy to escape from the lattice sites and move freely through the crystal.

When an incoming X-ray photon interacts with an electron in the valence band, the electron may absorb a significant amount of energy to be removed from its lattice site and be elevated to the conduction band. This leaves a single hole in the valence band, which will be filled when the electron, or any other electron, falls back into this position from the conduction band. The return of an electron to this state of lower energy results in the emission of a photon with energy equal to the energy difference between conduction and the valence band energies. The gap width between the valence and conduction bands therefore determines the energy of the produced photons. Small amounts of impurities, referred to as activators may be added to create special sites in the forbidden energy region between the valence and conduction bands to form smaller transition gaps between allowed electron energy levels (see Figure 2-6). The activators are chosen carefully to create sites at specific positions so that a transition from one of these sites to the valence band or to each other will produce photons with selected energies, detectable by the camera.

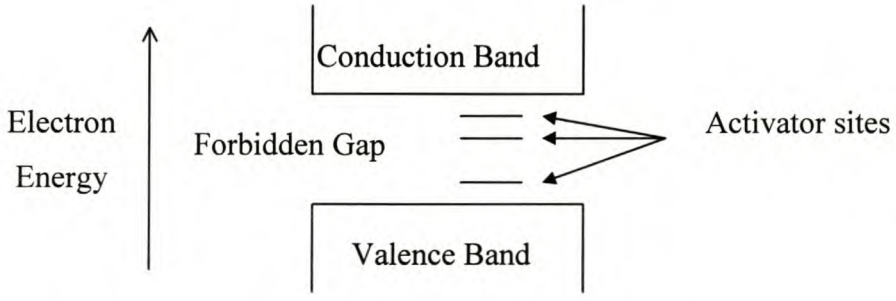

Figure 2-6: Electron energy levels in a crystal lattice of an inorganic scintillator.

2.4.2 Organic scintillators

In organic materials fluorescence is the result of de-excitation of a single molecule and does not depend on the structure of the crystal lattice or the physical state of the material. The fluorescence ability of organic scintillators is independent of the physical state of the material (from vapour to a solid form) as long as the molecular structure is preserved. Incident ionising radiation causes the production of secondary electrons, which in turn produce ionisation and excitation of molecules, which then lose their excess energy via decay to their original states by emission of light. Due to the low atomic number of organic scintillators and their consequent low light yield, organic scintillators are not used in radiology and will not be discussed further.

2.4.3 Scintillation screens for X-ray imaging

Scintillation screens were originally used to enhance the production of light to blacken radiographic film in order to reduce the X-ray dose given to patients. The wavelength of the light emitted from the scintillation screen is chosen to match the optimum sensitivity of the film for optimal use of the X-ray beam. This is also required for a digital system and the emission wavelength is chosen to fall in the range of wavelengths where detection efficiency of the CCD camera is high [Joh83]. CCD camera based digital imaging systems use a scintillator screen and mirror combination with the camera placed outside the beam (at a 90 ° angle), to avoid damage to the electronic circuits of the camera. Another advantage of using a scintillation screen is that the number of emitted photons can be calculated and kept below the saturation level of the pixels of the CCD camera to optimise the dynamic range of the CCD camera.

Calcium tungstate screens ($CaWO_4$) were originally used in screen-film combinations for its ultraviolet light spectrum, which is strongly absorbed in the film base material. These screens therefore give higher image resolution on film because of less diffusion and scattering in the film emulsion. Many other phosphor materials are being used for different applications, depending on their emission wavelength and scintillation efficiency. Rare earth phosphors have been used since 1973 because of their high absorption and conversion efficiencies. Two types of rare earth phosphors are commonly used, namely the green-emitting rare-earth oxysulphides (terbium activated) X_2O_2S:Tb, where X is gadolinium, lanthanum or yttrium and the blue and ultraviolet-emitting phosphors, lanthanum oxybromide LaOBr:Tm [Bar81], [Cur90].

The emission efficiency, emission wavelength and the screen density are important properties to consider when choosing a scintillator for a specific application.

2.4.4 Scintillation efficiency

The interaction of external radiation causes excitation of atoms or molecules, which will in turn decay and emit light. Only a small fraction of these decays will result in the emission of fluorescent light and a large amount of the energy passed to the scintillator is dissipated non-radiatively. The ratio between the energy emitted as visible light and the amount of energy deposited in the scintillator material is called the scintillation efficiency [Kno89]. The fraction of

the X-ray beam incident on the scintillator that does not contribute to the production of light is referred to as quenched radiation.

The scintillation efficiency for a scintillation screen depends on the absorption and the conversion efficiencies of the screen. Only a fraction of the X-ray beam incident on the screen is absorbed in the screen and the absorption efficiency gives an indication of the fraction (number of photons) absorbed in the screen. Furthermore, not all of the absorbed X-ray photons will be converted to light. The conversion efficiency refers to the ability of the phosphor material to convert X-rays to light and gives the ratio of light emitted by the screen to the amount absorbed in the screen.

The absorption efficiency depends on the type of interaction that takes place in the phosphor and therefore depends on the energy of the incoming X-ray photon. The probability for photoelectric absorption is higher for elements with high atomic number and for low energy X-ray photons, especially for photon energy close to the binding energy of an electron in the K-shell of an atom (see photoelectric absorption, section 2.3.2). Choosing a material with a high atomic number can therefore increase the absorption efficiency [Cur90]. The screen absorption is higher in the region of the absorption edge [Cur90]. The K absorption edges for rare earth elements fall in the diagnostic X-ray energy range and rare earth screens therefore have higher absorption efficiencies, even though the average atomic numbers of rare earth screen compounds are lower than for $CaWO_4$ [Cur90]. The absorption efficiency for rare earth materials is roughly twice as high as for calcium tungstate.

The conversion efficiency depends only on the phosphor and activator materials and is independent of the deposition density of the material. Calcium tungstate has a conversion efficiency of around 5 % and rare earth phosphors have much higher conversion efficiencies e.g. 19 % for ZnCdS:Ag [Ryn95], [Cur90]. If the conversion efficiency of a scintillator is known, the number of light photons emitted can easily be calculated from the amount of X-ray energy absorbed by the screen [Bo98a].

2.4.5 Screen speed, deposition density and resolution

The screen speed refers to the number of light photons created for each incoming X-ray photon. For film screen systems the screen speed is described as the X-ray exposure needed with and

without a scintillation screen respectively to produce the same image quality. This ratio is measured by the intensification factor, which is the ratio of exposure required without a screen to the exposure needed with a screen to obtain the same image quality or light yield, as measured with the CCD camera. Fast screens have high intensification factors [Mer79]. The screen speed depends on the thickness of the phosphor layer and on the conversion and absorption efficiencies.

Only a small fraction of the X-ray beam energy is converted to produce the light spectrum, but the number of resulting light photons is much higher than the number of X-ray photons incident on the screen [Mer79]. The luminous efficiency factor indicates the number of visible light photons emitted in relation to a single X-ray photon absorbed by the scintillator and is always greater than one.

Increasing the thickness of the phosphor layer is the easiest way to increase the screen speed, but thick screens have lower resolution [Bar81]. A thick layer of phosphor, i.e. more crystals, can absorb more of the same X-ray beam than a thin layer, which means that the beam is used more effectively but leads to the diffusion of light and a reduction in image sharpness. Light can be produced at larger distances from the screen surface and therefore be scattered more in a thicker screen [Cur90]. The screen speed is therefore closely related to the screen resolution and therefore the system resolution. There is always a compromise between speed and resolution, thus the screen is carefully selected for the specific application [Cur90].

At low energies, the probability for an X-ray photon to be photo-electrically absorbed is higher than the probability for Compton scattering (see Figure 2-5). Light photons are produced by secondary electrons resulting from one of these interactions. An X-ray photon absorbed through photoelectric absorption will produce a light photon close to the position where the photon is absorbed. However, light that is produced by an X-ray photon that has undergone one or more Compton scattering interactions before it is absorbed, will reduce the image sharpness, because of randomness of the interaction positions. The probability of absorption of a Compton scattered photon is higher for thick scintillators [Bar81].

The deposition density is a term used to specify the amount of fluorescent material deposited per unit area on the screen (mg/cm^2). The screen speed increases with increased deposition density because of the higher concentration of fluorescent material contributing to the production of light. This is because scintillators with high densities have higher absorption efficiencies because

of higher attenuation of the X-ray beam. Choosing a high-density phosphor is a more effective way of increasing the screen speed than increasing the screen thickness, since the contribution of diffusion of light in the phosphor and the uncertainty in interaction position of the incident X-ray photon are not increased.

The spatial resolution of film images is limited by the scintillation screen resolution, since films can record up to 100 line pairs per millimetre but the highest resolution screens can resolve only about 10 line pairs per millimetre.

2.4.6 Contribution to image noise

A scintillation screen with high conversion efficiency uses the X-ray beam more effectively and a lower X-ray fluence (number of photons per unit area) may be used to obtain the desired light yield. However, a lower fluence means that the average spacing between positions where X-ray photons interact in the screen is increased. If the spacing between adjacent interaction positions becomes larger than the dimension of the point spread function created by each photon, the image will appear grainy or mottled. This is known as quantum mottle. Quantum mottle is a result of statistical fluctuation in the number of X-ray photons absorbed by the screen and becomes visible when individual point spread functions are smaller than the spacing between incoming X-ray photons. The presence of mottle or graininess in an image makes it difficult to distinguish fine structures in an image [Bar81]

2.4.7 Scintillation crystal structure

The size and shapes of the scintillator crystals or the 'fineness' of powders in case of inorganic powders affect the image quality significantly. Most inorganic scintillation materials (such as Gd_2O_2S:Tb) are available as powders but are different in terms of the particle sizes or graininess and densities. Larger phosphor grains will result in a higher light yield, because of more effective X-ray absorption and conversion. A screen with bigger grains therefore has higher speed, but gives a 'less sharp' image than a screen with smaller grains. For bigger grains of scintillating material, the emission of light is more likely to be in all possible directions, rather than in the forward direction because of an added degree of freedom in the orientation of the crystals (large spacing between crystals). Although the light yield is lower with smaller phosphor grains, the grains are packed closer to each other (high deposition density), which means that a more

detailed picture (higher resolution) can be obtained with a screen composed of small grains (see Figure 2-7 (a)).

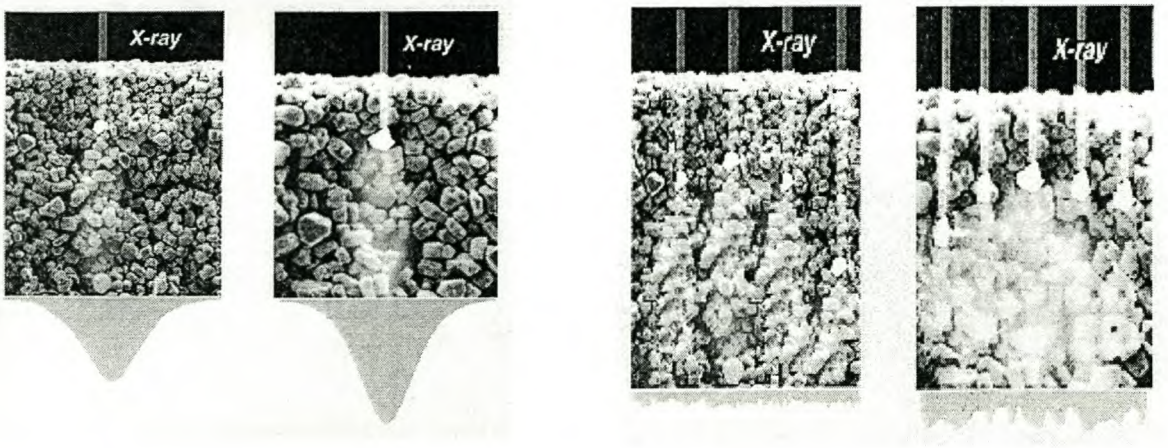

Figure 2-7 (a): Illustration of the effect of the phosphor grain size on the light intensity and resolution. (Images from Hamamatsu [Ham99]).

A scintillation screen that produces very high resolution is thallium doped caesium iodide CsI:Tl. CsI:Tl is an inorganic scintillator with cylindrical shaped crystals, which produces high resolution due to the collimated angular distribution of the light (see Figure 2-7 (b)). CsI:Tl has a very high light yield and broad emission peak at 550 nm (see section 2.4.8 for definition of the emission spectrum), which lies in the high sensitivity wavelength range of the camera [Bic99]. The CsI:Tl scintillation screen is suitable for this digital system but is very expensive compared with other scintillation screens, since it is composed of crystals grown onto a substrate.

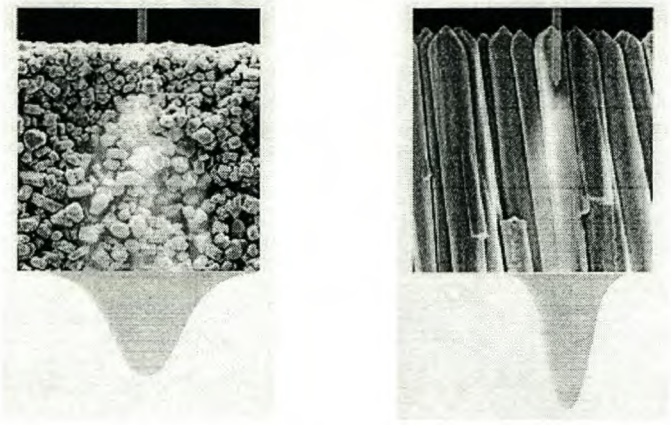

Figure 2-7 (b): Illustration of the affect of the crystal structure on the screen resolution. Left: grainy structure Gd_2O_2S:Tb powder. Right: cylindrical crystals of CsI:Tl. A higher resolution can be obtained with the needle shape crystals of CsI:Tl Images from Hamamatsu Photonics [Ham99].

Light photons produced in the scintillation screen will be emitted in different directions [Cur90]. This contributes greatly to the spreading of light produced at a point [Gia85]. The reflection of the emitted light by the mirror also causes spreading of the light. The light can also be reflected back to the scintillation screen and be re-emitted from the screen. This scatter contribution to the decrease in resolution is lower for points where the mirror is far away from the screen.

2.4.8 Emission spectrum

The emission spectrum for a screen indicates the relative intensity of light emission for different wavelengths. Calcium tungstate has a broad emission spectrum with emission peak around 430 nm [Cur90]. The emission spectrum of Gd_2O_2S:Tb is a line spectrum with a strong emission peak at 545 nm. The emission peak represents the wavelength of light that has the highest percentage of emission by the screen. The emission peak wavelength of the scintillation screen should match the maximum quantum efficiency wavelength of the CCD chip to ensure the highest light sensitivity for the system (see sections 3.3.1 and 3.3.2).

2.5 CCD camera theory

A CCD (charge coupled device) camera captures the optical image from the scintillation screen and converts it to an electronic or digital image. W S Boyle and G G Amelio invented the charge-coupled device in 1970 at Bell laboratory in Orlando. The phrase charge coupled device, or charge transfer device, refers to the techniques used to transport the charge (electronic image) through the system, as will be explained in section 2.5.3 (charge read-out).

CCDs are notably replacing the commonly used vidicon vacuum tube TV cameras for the capture of digital images and are also widely used in electronic devices where storage and transport of charge is required. A charge coupled device used for creating a two dimensional image consists of a solid state array of silicon diodes, called photosites or pixels. These pixels are sensitive to visible light and convert light that falls onto it to an electronic signal proportional to the amount of incident light [Gon93]. An understanding of how the light is captured and how the signal is digitised and transported to a digital computer will be acquired from a closer look at the working of a charge-coupled device.

2.5.1 The working of a charge coupled device (CCD)

The detection of optical photons by a charge-coupled device may be explained by an examination of the principles behind a metal-oxide-semiconductor (MOS) capacitor. A MOS capacitor consists of a semiconductor substrate, normally p-type, with an n-type semiconductor layer to form a diode. Silicon and germanium are commonly used semiconductors, of which silicon is best suited for capturing visible light and is used in most CCDs. A brief explanation of the relevant semiconductor physics is given below.

Silicon is often used in semiconductor applications, especially CCD imaging applications and will be used as an example to illustrate the working of a CCD.

Silicon has four electrons in its highest energy level. Each silicon atom forms a covalent bond with four neighbouring atoms to form a neutral semiconductor crystal. If pure silicon is doped with a material from group five in the periodic table, with one more electron in its outer energy level, for example arsenic, a number of silicon atoms can be replaced by arsenic atoms adding unbound electrons to the crystal structure. These electrons can easily be excited to form part of

the conduction band and are called donors, with arsenic the donor material. The silicon now has additional free electrons (negative charge carriers) and is called an n-type semiconductor. Similarly, a p-type semiconductor is formed when a material from group three in the periodic table, with one less electron in its outer energy level, is added to pure silicon. This bonding will leave a "positive hole" (positive charge carrier) in the structure, which may be filled by electrons from the valence band of neighbouring atoms.

When p-type and n-type materials are connected, electrons will migrate from the n-type semiconductor to the p-type semiconductor and the holes effectively migrate in the opposite direction. Electrons entering the p-type material will combine with the holes and leave a net positive charge behind. Similarly, the holes migrating into the n-type material combine with the electrons and leave a net negative charge at the p-type side. The region directly adjacent to the p-n-junction over which the charge migrates is called the depletion region. The depletion region has an opposite polarisation from the surrounding semiconductor materials, which stops further migration of charge into the region and a state of equilibrium is reached. The amount of charge that migrated over the p-n-junction determines the width of the depletion region and therefore the potential over the junction. With equilibrium established, there is no net movement of charge inside and through the depletion region. The depletion region is therefore effectively a capacitor with potential determined by the migrated charge and the separator distance equal to the width of the depletion region.

2.5.2 Charge coupled device structure

A charge-coupled device is composed of a semiconductor substrate, generally p-type, covered with an n-type semiconductor of about 1 μm thickness (to form a p-n-junction) and a metal or heavily doped silicon layer or electrode as illustrated in Figure 2-8. By connecting the top silicon layer to a positive electrical potential, i.e. connecting the p-n junction in reverse bias, the depletion region is enlarged and serves as a potential well where the electrons are collected. Free electrons will accumulate at the potential well, since the well is at a higher potential and therefore has a lower potential energy:

$$E_p = -|q|\, V, \tag{2-9}$$

where E_p is the potential energy and V the electric potential experienced by a particle with charge q, which is an electron in this case. Electrons created in the region close to the well will move

towards the well and will also be stored there. The electron capacity of the potential well is of the order of 10^6 electrons.

This type of charge coupled device is referred to as a buried channel capacitor, since the channel is beneath the silicon dioxide surface (see Figure 2-8). Another type of CCD is the surface channel, but the buried channel is easier to manufacture and has more applications.

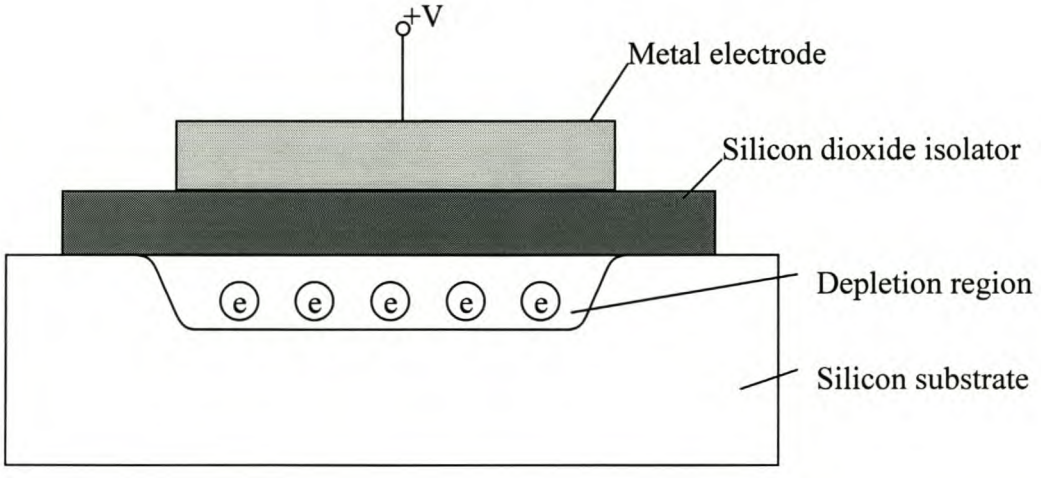

Figure 2-8: Charged coupled device (buried channel MOS capacitor).

The CCD chip is an array of many of these CCD elements, called pixels. Typical CCD configurations are interline-transfer and full-frame transfer CCDs. The full frame transfer CCD chip holds two identical imaging areas. After charge integration in the imaging array, the whole electronic image is moved to the storage array so that the next image can be captured by the imaging array. A full frame CCD can therefore have a high shutter speed. The storage area of an interline transfer CCD is between the columns of the exposed pixels, and not a separate array of pixels. Interline CCDs therefore have lower sensitivity because of the inactive or dead space between adjacent pixels and smaller pixel size for the same size chip and therefore also a lower full well capacity and dynamic range.

Photons incident on a pixel of the silicon CCD chip, will photo electrically create free electrons (generate electron-hole pairs) [Fah95]. The electrons are free to migrate and will move to the potential well and the holes will be collected in the p-type substrate. Electrons will collect in the potential well until it is saturated and will then spill over to a neighbouring pixel. The number of electrons collected in a pixel is proportional to the number of photons falling onto the chip, i.e.

the light intensity and the exposure time, but non-linearly dependent on the wavelength. The optical image projected onto the array of pixels is therefore an electronic copy of the original light image with its varying light intensities. Each value in the image array of charge quantities is converted to a voltage proportional to the amount of charge in each pixel. The voltage is amplified, digitised and read out as a stream of data.

2.5.3 Charge read-out

The read-out is performed by a programmed sequence of changing the gate potentials of neighbouring pixels. There are various pixel configurations, according to the number of external electrodes or gates (see Figure 2-9). Two and three connectors are more commonly used and referred to as two and three phase technology respectively. The read-out process for a two-phase CCD array is described below and illustrated in Figure 2-9 and Figure 2-10.

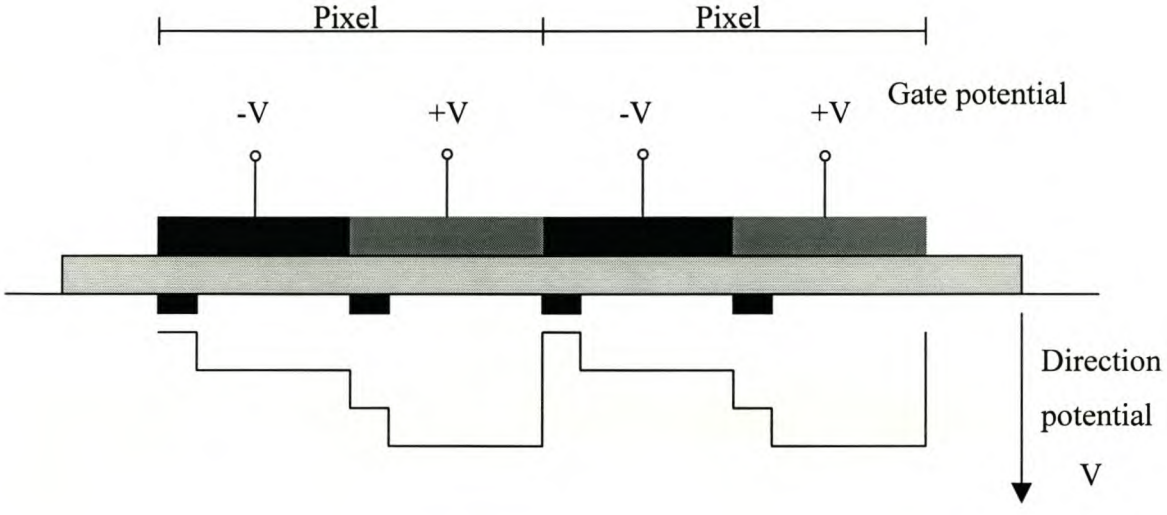

Figure 2-9: Cross section through two pixels of a two-phase CCD [Kod92].

The gate potential forms the boundaries of a pixel and serves as isolation for the charge collected in each pixel from neighbouring pixels (see Figure 2-9). During integration, both V1 and V2 are kept low and charge is collected in the whole region below V1 and V2 (see Figure 2-10). During the first step of charge transfer, V1 is increased, and the charge from V1 and V2 collects below V1. After the charge has been collected below V1, V1 and V2 are reversed so that the charge below V1 moves to V2, shifting the entire row down towards the horizontal CCD. All rows are

moved down one step at a time and each time the charge in the last row is moved into the horizontal register. The pixels in the horizontal register are transferred to the output node as individual charge packets, similarly to the way the rows of charge are moved down. The charge in each packet is converted to voltage by an amplifier at the output node where the charge leaves the horizontal shift register (output amplifier). The output amplifier performs the charge-to-voltage conversion and amplifies the signal linearly, which produces a signal proportional to the amount of charge in each packet.

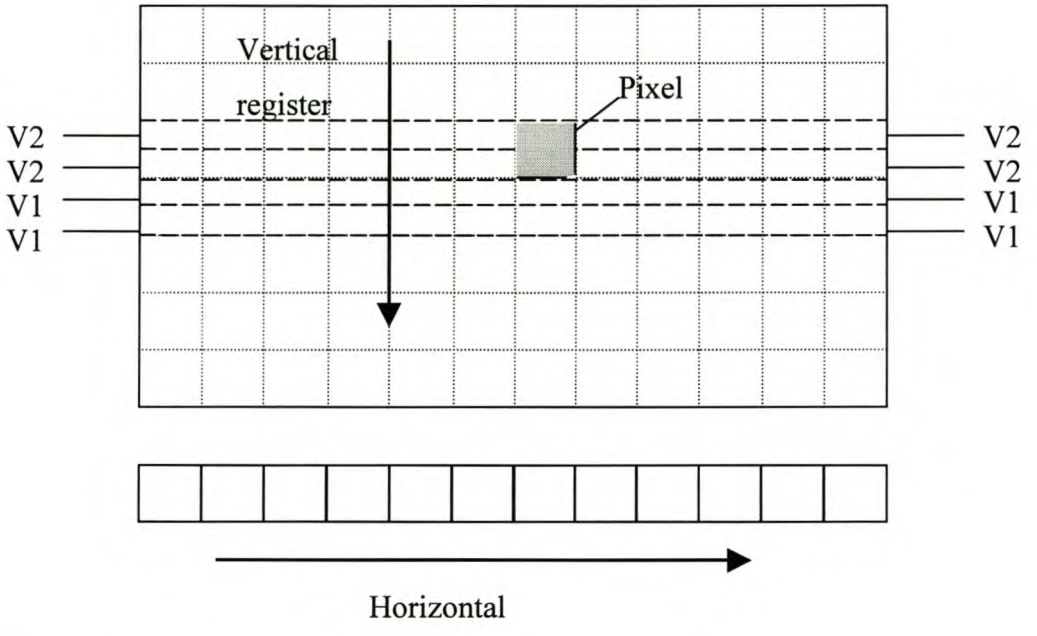

Figure 2-10: CCD pixel array illustrating the direction of charge transport during read-out.

To summarise, the read-out of the pixel array occurs in two steps: after the charge is collected in all pixels, the rows of pixels are first shifted down, row by row and then read out pixel by pixel at the end of the last row. The individual pixels that reach the output node of the horizontal register are digitised and combined as an array of digital image values.

The charge transfer efficiency (CTE) of a CCD is a parameter that indicates the efficiency of the charge transfer, since some electrons are normally 'lost' during read-out. The charge transfer efficiency depends on the design of the CCD chip.

Pixel binning refers to the joining of charge in adjacent pixels during read-out to obtain higher signal levels, i.e. higher signal-to-noise ratio. While the dynamic range of the CCD is almost doubled, the resolution is halved (in one direction), and binning is only used where sensitivity is more important than resolution.

2.5.4 Peltier cooling of CCD chip

Peltier cooling or thermoelectric cooling is used to reduce the contribution of thermal electrons during charge collection by cooling the CCD chip (see section 2.7.1 for the definition of dark current).

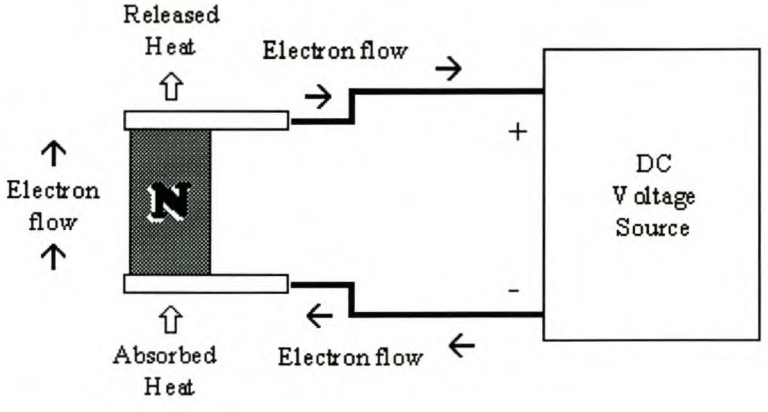

Figure 2-11: The direction of heat transfer during Peltier cooling.

Peltier cooling is based on the principle of the absorption or production of heat at the junction of two different conductors in an electronic circuit, depending on the direction of flow of the current. A semiconductor material is attached to a conductive material and connected to a power supply unit. If the voltage source is connected over the junction, charge carriers will move through the junction towards the positive electrode. The charge carriers transfer heat to the neighbouring material. If an n-type material is used (see section 2.5.2), the charge carriers are the electrons. As the electrons enter the n-type material (as shown in Figure 2-11) heat is absorbed and then transferred through the n-type material to the distant end and then released. A p-type material is often used instead of an n-type material, while the charge carriers are positive 'holes' instead of electrons.

2.5.5 Quantum efficiency, dynamic range and linearity of the CCD camera

The quantum efficiency of a CCD is the ratio of the number of photoelectrons produced to the number of photons incident upon a detector. CCDs normally have quantum efficiencies of about 50 % or greater at visible wavelengths (see Figure 3-3). Since the light yield is non-linearly dependent on the wavelength, the quantum efficiency is specified for different wavelengths, called the spectral response of the CCD

The dynamic range of the CCD camera is the difference between the maximum and minimum pixel values in an image. It is expressed as the ratio of the amplitude of the highest measurable signal to the smallest meaningful signal. The highest signal is determined by the electron capacity of each pixel. The detectability of low signals is limited by noise inherent of the system, also often called the noise floor. The dynamic range is increased if the intrinsic detector noise is kept low (see Figure 2-12).

The dynamic range is normally indicated in decibels, as the ratio of the well capacity over the noise level of the system:

$$\text{Dynamic range} = 20\log_{10}\left(\frac{\text{Well capacity}}{\text{Intrinsic detector noise floor}}\right)\text{(dB)} \qquad (2\text{-}10)$$

The unit decibel is defined for expressing the relationship of two power signals:

$$\text{Power difference in decibel} = 10\log_{10}\left(\frac{\text{Power of signal A}}{\text{Power of signal B}}\right)\text{(dB)} \qquad (2\text{-}11)$$

Since the dynamic range is measured as voltage values rather than power, the relationship in decibels becomes $P = 20\log_{10}\left(\frac{\text{Power of signal A}}{\text{Power of signal B}}\right)$ (dB), because $P = \frac{V^2}{R}$ and the square inside the logarithm becomes a multiplication with two.

The dynamic range gives an indication of the digitisation level that is preferred for the system. A large well capacity will have a larger dynamic range, but also a bigger contribution of noise (more electrons per pixel contributing to noise). The number of electrons per digitisation level should be kept low (see read-out noise, section 2.7.1).

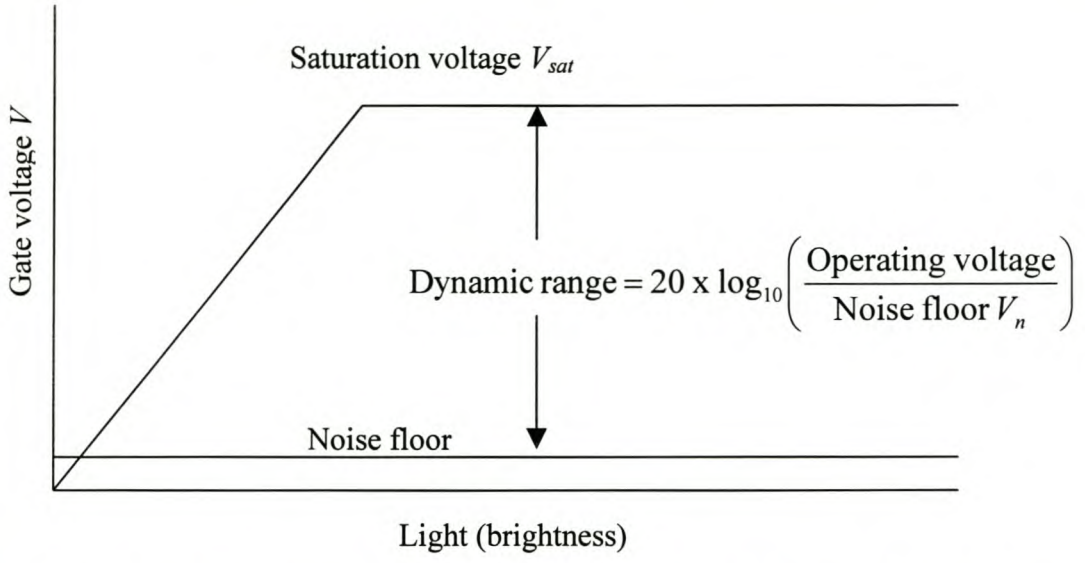

Figure 2-12: Graph of the gate voltage vs. illumination. As the gate voltage is increased, the amount of light that can be stored in a pixel is also increased, until the saturation voltage is reached when the well capacity is exceeded.

CCD response should be linear over the full dynamic range, which means that there should be a linear response between the number of X-ray photons and the number of electrons they produce.

The dynamic range is often specified in terms of the number of grey scale levels provided by the analog to digital converter. An analog to digital converter with b bits has 2^b available grey scale levels (see quantisation, section 2.5.5)

2.5.6 Analog-to-digital conversion: sampling, quantisation and coding

The CCD camera produces an electronic signal corresponding to the optical image that is transformed to a digital image by analog-to-digital conversion. This conversion involves sampling of the image, quantisation of the values and coding of the discrete values. Sampling of the image is a result of the finite pixel size, since the image is divided into an array of values according to the pixels on the CCD chip. The pixel values are read out as voltage signals that have to be converted to a number (digitised) and represented by a computer (coded).

The light image emitted by the scintillator screen is focussed onto the array of pixels of the CCD chip. The analog image is therefore projected onto a set of discrete intervals, just as a continuous function can be sampled at discrete intervals to produce a discrete representation of the function. A sampled image is a representation of the values of an analog image at discrete position intervals. The CCD pixels take on the values of the analog image at the corresponding points in the image, which are then referred to as the sampled values.

The sampling rate or sampling frequency F_s specifies the number of values that are obtained from the analog signal per interval. For time signals the interval is a time period and the sampling rate is expressed as samples per second. For images the interval is length or distance and for a sampling interval expressed in millimetres, the sampling rate will be expressed as samples per millimetre.

The sampling rate holds important information about the contents of the digital image. If too few values of the analog image (samples) are used to represent the image, information will be lost and the image will not be translated accurately. High frequency components in the image have to be sampled at a high rate, i.e. with a high sampling frequency, to be represented accurately in the digital image. The high frequency components therefore determine the minimum rate at which the image should be sampled to obtain a desired degree of accuracy.

The sampling frequency for a CCD camera is determined by the pixel size of the CCD chip. The pixel size, also called the sampling distance, therefore determines the Nyquist frequency which is the minimum sampling frequency required to resolve a structure with a certain frequency [Pro96], [Dro85]. If a picture is sampled at a frequency lower than the Nyquist frequency, the fine, high frequency structures in the image will not be recorded correctly by the system and image detail will be lost. According to the sampling theorem, an image sampled at a frequency higher than twice the highest frequency contained in the image can be exactly recovered from its sampled values. This means that the Nyquist frequency should be slightly higher than twice the highest frequency in the image [Pro96]. In this case there will be no loss of information and the original image can be perfectly recovered from its sampled representation.

The Nyquist frequency is also defined as $\frac{1}{2\Delta x}$ where Δx is the sampling distance [Fuj85] (see spatial resolution, section 2.7.5).

When the sampled image is converted to a complete digital form, the image values obtained by sampling have to be represented by a finite number of digits. An analog to digital converter divides the voltage from each pixel into a range of levels or intervals and assigns a value to each interval. This is called quantisation or often referred to as digitising since the value will be represented by a finite number of digits or bits in a computer. Each quantisation step corresponds to one bit and the total number of available bits determines the range of quantisation levels. The digital resolution, a term often used to describe the quantisation, refers to the number of bits provided by the analog-to-digital converter of the CCD camera used for digitisation. A digital resolution of b bits corresponds to 2^b digital values.

Unlike sampling, quantisation is an irreversible process, since many distinct values in the same interval are given the same value. However, the digitisation error is fairly small if a large number of bits are used, as explained below (see equation 2.14).

Quantisation introduces distortion of the image because the exact pixel values are rounded or truncated to the nearest digital interval level. The difference between the continuous image value and the digitised value is given by the quantisation error or quantisation noise. This error is proportional to the quantisation step size, since small steps will lead to a smaller deviation from the original value.

The quantisation error is normally evaluated for sinusoidal signals because they are used as test signals in analog to digital converters. The ratio of the signal power to the noise power gives the signal-to-quantisation noise ratio (SQNR) [Pro96]:

$$\mathrm{SQNR} = \frac{P_i}{P_q} \tag{2-12}$$

The SQNR is calculated as

$$\mathrm{SQNR} = \frac{P_i}{P_q} = \frac{3}{2} \cdot 2^{2b} \tag{2-13}$$

or expressed in decibels:

$$\mathrm{SQNR(dB)} = 10 \log_{10} \mathrm{SQNR} = 1.76 + 6.02b \tag{2-14}$$

with b the number of bits used by the A-D converter (see Appendix A for the derivation). This result illustrates that the SQNR increases by 6 dB if the number of bits is increased by one.

Coding concerns the representation of each value in a computer by binary sequences. Coding offers no direct way of improving the quality of a digital image but is often used to compress the size of image files (see image file formats, section 2.8.3).

2.6 Optical system

The light image from the scintillation screen is focussed onto the CCD chip by an optical system, consisting of the mirror and lens. The optical part of the system influences the light collection and therefore the total light yield of the system and also plays an important role in the image quality in terms of the resolution, distortion and scatter. The characteristics of an optical system and how it influences image formation will be considered in this section.

2.6.1 Optical principles and definitions

The optical terms and definitions used to describe the performance of the optical system are the working distance, field of view, lens quality (numerical aperture) and the depth of field.

The working distance of a lens is the minimum object distance for which a sharp real image can be obtained. The field of view is the object area that is focussed onto the chip. The field of view influences the amount of light collected by the camera and therefore the sensitivity of the system. It is shown in section 2.7.5 that the field of view determines the system resolution. The lens diaphragm diameter or aperture size determines the amount of light that passes through the optical system. The F-number or F-stop of a lens, F, is defined as the focal length of the lens f divided by the aperture diameter ϕ:

$$F = \frac{f}{\phi} \tag{2-15}$$

A parameter used for expressing the quality of a lens is the numerical aperture, $N.A$, defined as

$$N.A = \frac{\phi}{2f} = \frac{1}{2F} \tag{2-16}$$

A high quality lens has a low numerical aperture or high F-number (small aperture). The light yield is directly affected by aperture diameter and a lens with a large aperture is used to obtain the highest possible light yield. The lens quality is often compromised to obtain high light yield. The lens quality is usually higher in the middle of the available range of F-stops.

Light rays emerging from a single point are not perfectly projected to a single point in the image, but are spread out over a finite area in the image. As a result the images are blurred and this effect is referred to as aberration. The different kinds of aberration that have to be considered are spherical aberration, curvature of field and distortion. Spherical aberration occurs because light rays close to the central axis of the lens are focussed at a further distance than light passing near the outer edge of the lens, as illustrated in Figure 2-13. This causes peripheral blurring around the edges of the image because the image is projected onto a spherical surface, but viewed on a flat surface. If the image is in focus at the centre, it will be out of focus around the edges and vice versa. Spherical aberration is affected by the focal length, aperture, shape and object position.

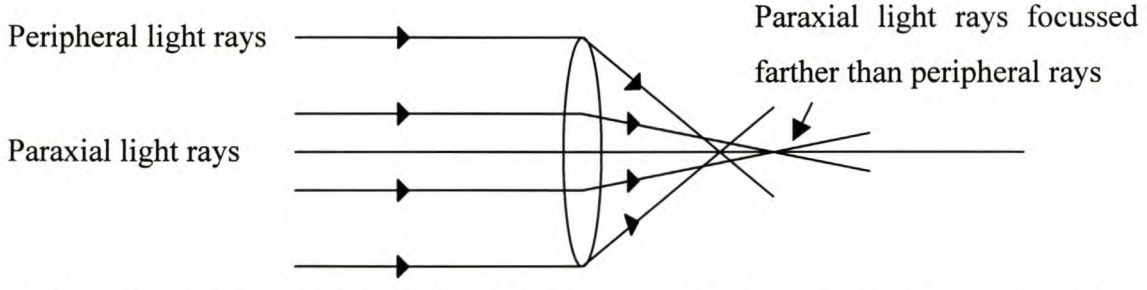

Figure 2.13: Illustration of spherical aberration: paraxial rays are focussed further than peripheral rays.

Curvature of field, also referred to as the fish eye effect, is also a result of the spherical shape of the lens causing point objects far from the optical axis of the lens to be formed at different depths than points close to or on the axis. This has the effect that the edge of the picture is out of focus when the image is sharply focussed in the middle. The effect of field curvature is related to the shape of the lens and the index of refraction and can therefore be reduced by choosing a suitable lens.

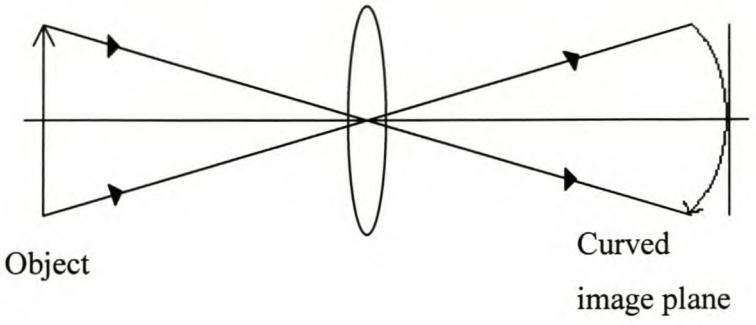

Figure 2-14: Curved image plane (fish eye effect).

An image is distorted when an object point is not projected to an image point position as calculated with the lens equation, but displaced from this position. Image points are therefore displaced with respect to each other. The effect of distortion is higher for points further away from the middle of the image. Distortion does not influence the resolution of the system, only the appearance of the image.

Another effect is the decrease of light collection at the peripheral edges of the image, referred to as vignetting [Bo98a], [Spr93]. Vignetting is larger for large aperture lenses (small field depths), short focal lengths and short object distances [Spr93].

The lens speed is defined as the maximum amount of light that is transmitted through the lens, which is obtained with the lowest F-number of the lens.

2.6.2 Depth of field (DOF)

The depth of field refers to the degree of freedom of object movement on the lens axis for which the image is still in focus. If the point object focussed at is in focus, the range of points just in front and behind it will only be partially in focus. Point objects outside the range of focus will be viewed as circles instead of points. If a point object position moves relative to the position where it is in focus, the image position will also move relative to the CCD chip. The point will be viewed as a circle with diameter proportional to the amount of axial movement from the sharply focussed position. The biggest acceptable circle for which the point will still be identified as a point is called the circle of confusion. The circle of confusion is illustrated in Figure 2-15

[Bar98]. The circle of confusion is therefore a measure of the image sharpness. As the object moves out of focus, the circle of confusion increases until the object is completely out of focus. The depth of field and circle of confusion are therefore closely related, and the circle of confusion restricts the field depth. The largest acceptable circle of confusion (for which the image is still sharply focussed) determines the field depth and has to be specified before the field depth can be quantified.

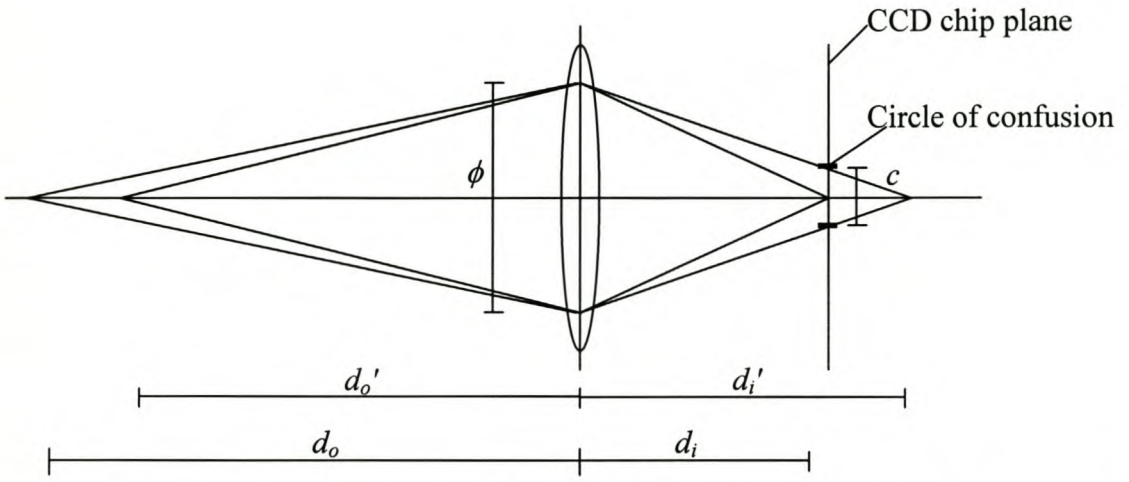

Figure 2-15: Graphical illustration of the circle of confusion. For a point object at d_o, a sharp image is formed at d_i on the CCD chip. If the object is moved to d_o', the image is formed at d_i' and the point object is seen as a circle since the CCD chip position remains unchanged at d_i. This is called the circle of confusion.

An expression for the field depth can easily be derived in terms of the circle of confusion, from the geometry in Figure 2-15, since

$$\frac{|d_i'-d_i|}{c} = \frac{d_i'}{\phi} \tag{2-17}$$

and therefore

$$|d_i'-d_i| = \frac{cd_i'}{\phi}, \tag{2-18}$$

where c is the circle of confusion, ϕ the lens diameter and d_i and d_i' the image distances of the object in focus and out of focus respectively; d_i' can either be smaller or bigger than d_i.

The image distance can be written in terms of the object distance d_o and the focal length f of the lens, using the lens equation:

$$d_i = \frac{d_o f}{d_o - f} \tag{2-19}$$

If c is the largest tolerable circle in the image plane, then $|d_o - d_o'|$ is the field depth, or the boundaries for the range of object distances that will form sharp images:

$$\text{DOF} = |d_o - d_o'| = \frac{c d_o'}{f\phi}(d_o - f) \tag{2-20}$$

On the right hand side of equation 2-20, d_o' can be replaced by d_o, since $|d_o - d_o'|$ is small compared with the object distance d_o. With the aperture diameter ϕ replaced with $\phi = \frac{f}{F}$ (Equation 2-15), the depth of field is then given by

$$\text{DOF} = |d_o - d_o'| = \frac{c d_o F}{f^2}(d_o - f) \tag{2-21}$$

The depth of field is therefore proportional to the circle of confusion. Equations 2-20 and 2-21 show that the depth of field is also proportional to the object distance (see Figure 2-16) and inversely proportional to the aperture size (see Figure 2-17) and focal length. The value for the circle of confusion sets the field depth boundaries. A realistic value for the circle of confusion for which the image appears to be in focus should therefore be chosen. If the value of the circle of confusion, measured in millimetres, is divided by the size of one pixel on the CCD chip, the picture sharpness can be expressed in terms of the number of pixels onto which a single point is spread out $\frac{c}{\text{Pixel Size}}\frac{[\text{mm}]}{[\text{mm}]/[\text{pixels}]}$ [Bar98]. The size of the circle of confusion also depends on magnification and display of final image. If we require at least three pixels to produce an image of a point, the circle of confusion is spread out over three pixels and the size of the circle of confusion (in millimetres) is given by

$$c = 3 \times \text{Pixel Size} \ \ [\text{mm}]. \tag{2-22}$$

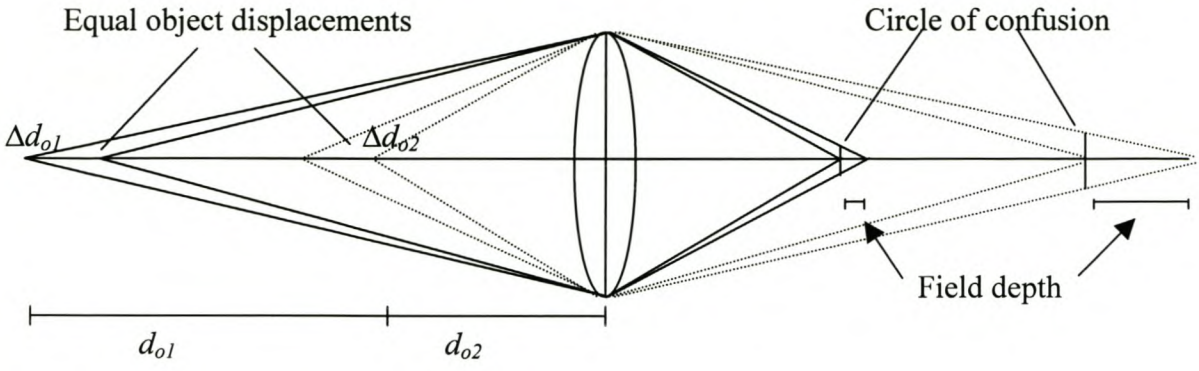

Figure 2-16: The depth of field is directly proportional to object distance. This figure illustrates the difference between equal object displacements ($\Delta d_{o1} = \Delta d_{o2}$) for different object distances ($d_{o1} >> d_{o2}$). For equal displacements, an object far away has a smaller circle of confusion i.e. more freedom of movement before the image is out of focus and therefore larger field depth.

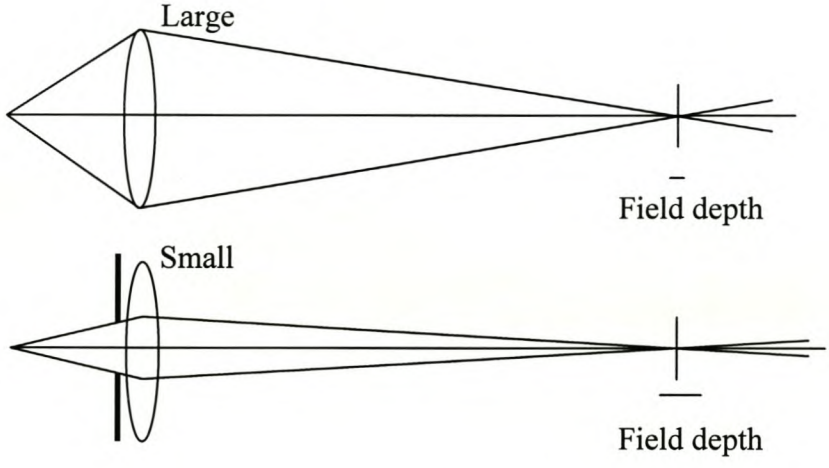

Figure 2-17: Illustration of how aperture size affects the depth of field – a small aperture size produces a large field depth. The lens aperture therefore not only affects the amount of light but also the field depth.

2.7 System performance

Digital imaging system performance is expressed in terms of the system noise, light yield and total spatial resolution. Various parameters are used to express the properties as quantities that can easily be compared with other systems. The most important parameters are the light yield, signal-to-noise ratio, detective quantum efficiency and the contrast transfer through the system (as measured by the modulation transfer function).

2.7.1 Noise

Noise is the unwanted random contributions to an image, caused by non-repeatable random signals from various sources. Noise in the system limits the detectability of low contrast structures. The primary sources of noise are the X-ray quantum noise, CCD chip contributions and digitisation noise [Mu90a]. The X-ray quantum noise is a result of the quantified nature of X-ray imaging and its effect is small for large numbers of X-ray photons (i.e. large exposures), see section 2.4.6 (scintillator contributions to noise). The digitisation noise is caused by the digitisation or rounding error, when a digital value is assigned to a measured voltage, see section 2.5.5 (quantisation error). Noise from the CCD chip is added during charge accumulation from the production of thermal electrons (thermal noise), or during read-out of the image, when electrons are added to or lost from pixels during read-out of the image (read-out noise).

The system noise contribution can be measured by the noise power spectrum NPS of the detector. This spectrum is obtained from the variation of the image signal from its average value, as a function of spatial frequency [Mu90b].

Apart from the electrons created by light photons falling on to the CCD chip, there are other sources of electrons that only contribute to noise in the image. The biggest noise source from the CCD chip is the creation of thermal electrons in the CCD. Thermal electrons are created in the absence of light when the CCD heats up and electrons in the semiconductor gain enough thermal energy to escape from their bound sites and contribute to the signal. This noise is inherent to the system and is referred to as dark current. The dark current contribution increases with temperature and can therefore be minimised by cooling the CCD chip.

When the image is transported to the output node on the CCD chip, electrons are removed from or added to pixels, known as read-out noise. After the image has been read out, the charge signals from the pixels are first converted to voltages and then amplified and digitised according to the number of quantisation levels (determined by the number of bits used). The digital signal is then read out as analog-to-digital conversion units (ADU). Errors in reading the signal caused by the on-chip amplifier also contribute to the read-out noise. The CCD chip is primarily responsible for the read-out noise and the contribution from other parts of the digital system is very small.

2.7.2 Light yield

The light yield of a digital imaging system refers to the number of visible light photons detected by the camera, or the CCD signal strength relative to the number of X-ray photons incident on the scintillator screen. The total light yield obtained with the digital system is affected by nearly all the components of the system: the X-ray beam, scintillator screen, lens and CCD camera. The individual components should be carefully selected in order to optimise the light collection through the system to preserve high image quality and to ensure low patient dose.

The number of X-ray photons as well as the photon energy determines the number of light photons produced in the screen. The emission efficiency of the scintillator material and screen thickness determine the production of visible light photons. The emission efficiency depends on the absorption and conversion efficiencies, which are properties of the scintillator material as given in section 2.4.4 (scintillation efficiency). The scintillator cassette or screen backing attenuates the X-ray beam and does not necessarily contribute to the light yield. High energy X-ray beam imaging systems often use a metal plate to enhance the light yield as electrons resulting from Compton scattering in the metal plate will be stopped in the scintillator [Alt96], [Bo98a], [Har88]. The diagnostic X-ray energy range only reaches up to 150 keV where photoelectric absorption dominates, especially for high Z-numbers. For these low X-ray energies, materials with high density and atomic number will only attenuate the X-ray beam without contributing to the light yield. A material with low atomic number is therefore used as screen mounting.

The optical coupling efficiency or collection efficiency gives an indication of the amount of light lost between the scintillator and the CCD chip. Using a large aperture lens and short set-up distances can increase the total optical coupling efficiency. The coupling efficiency also depends on the emission characteristics of the scintillation screen [Yut97].

The well capacity of a pixel on the CCD chip determines the maximum amount of charge that can be collected and therefore puts an upper limit on the light yield.

The angular distribution of the light emitted by the scintillator will affect the number of photons that fall onto the CCD chip [Kno89]. The light distribution from a non-transparent scintillator is assumed to be Lambertian [Bo98a], [Liu94]. The light intensity for a Lambertian distribution obeys Lambert's law, which states that the intensity in a specific direction varies as the cosine of the angle between that direction and the normal to the surface. However, Giakoumakis and Miliotis [Gia85] have shown that the angular distribution of light emitted by non-transparent fluorescent screens differs considerably from a Lambertian distribution, and that calculations of the light flux and screen efficiency are influenced considerably by this error. The distribution differs from a Lambertian distribution due to attenuation of light in the scintillation screen, and is peaked in the forward direction [Liu94]. The screen density and the phosphor grain size also affect the angular light distribution, while the emission and absorption spectra of the screen and the angle of X-ray beam incidence on the screen do not significantly influence the angular distribution [Gia85].

Light passes through the lens after being reflected from the mirror and is focussed onto the array of CCD pixels. The camera will capture only light emitted in the forward direction from the scintillator falling within the solid angle subtended by the lens. The optical solid angle ω is given by

$$\omega = \left[\frac{\pi}{4}\frac{m^2}{F^2(1+m)^2}\right]\frac{1}{4\pi} \tag{2-23}$$

where m is the lens magnification and F the F-number of the lens [Bo98a].

The amount of light absorbed in the lens is expressed in terms of the transmission efficiency of the lens [Alt96].

Vignetting is the decrease of light collection at the edges of the image and plays a significant role in the loss of light at the edges of an image, specifically for short object distances [Cur90]. The lens quality determines the amount of vignetting, which is smaller for high quality lenses.

The quantum efficiency of the CCD chip gives a measure of the number of electrons generated in the chip by the incoming light, i.e. the conversion of optical photons into electrons (see section 2.5.4). The photon energy as well as the CCD chip material determines photon interactions in a material. The quantum efficiency is therefore different for all materials and is wavelength dependent (see Figure 3-3 in section 3.3.2). The well capacity of a pixel on the CCD chip determines the maximum amount of charge that can be collected and therefore puts an upper limit on the light yield.

2.7.3 Signal contrast ratio and signal to noise ratio

The image quality is dependent on the signal intensity and also the amount of noise in the system. The signal to noise ratio is the ratio of the signal strength relative to the noise limiting the signal detection. The image quality therefore increases as the signal to noise ratio is increased, which may be achieved either by increasing the dynamic range or a reduction in the system noise (see dynamic range, section 2.5.4).

The signal to noise ratio for a background signal is given by $\mathrm{SNR} = \frac{S_{BG}}{\sigma_{BG}}$ where S_{BG} is the background signal value and σ_{BG} the background noise, the standard deviation of the background signal [Alt96].

The signal to noise ratio is often measured by the ratio of the difference between an image value and its background to the noise in the system [Boy92], i.e.

$$\mathrm{SNR} = \frac{|s\text{-}s'|}{\sqrt{s+s'}} \tag{2-24}$$

where s is the signal value and s' the background.

2.7.4 Detective quantum efficiency

The detective quantum efficiency DQE gives an indication of the image quality and the detectability of objects in terms of the noise and contrast performance of the system.

The DQE is defined as $[(SNR)_{out}/(SNR)_{in}]^2$ where SNR_{out} indicates output signal to noise ratio of the radiation detector and SNR_{in} the signal to noise ratio associated with the radiation beam [Mu90b].

2.7.5 Spatial Resolution

The spatial resolution of an imaging system refers to the finest detail that can be resolved by the system. The spatial resolution, expressed in line pairs per millimetre, can be measured with a test object or by the modulation transfer function (MTF). A test object consisting of a series of regularly spaced bars and spaces (of known intervals) will give an indication of the maximum resolution that can be resolved with the system (see Figure 2-19 below, in section 2.7.6). The modulation transfer function indicates the contrast transfer of an image through the system at different frequencies [Mer79] (section 2.7.6). Measurement of the MTF is a more effective method for determining the resolution properties of the system than using a test object and also gives an indication of the sharpness of images [Cou81]. The MTF combines the two most important factors of imaging namely the measure of spatial detail and the preservation of the detail through the system as well as the maximum resolution of the system [Cou81].

The overall resolution of the digital imaging system is affected by all the parts of the imaging system, from the attenuation of the X-ray beam in the radiological object to the CCD camera. To minimise the total loss in resolution, all the factors have to be considered and their effect should be kept as small as possible. The MTF of the system can be obtained from the MTFs of the individual parts of the system.

The geometry of the imaging set-up plays an important role in image formation and therefore in the spatial resolution. The geometry concerns the focal spot size, the source distance and magnification. The contribution of the geometry to image sharpness is often described in terms of the penumbra. The penumbra, also called the edge gradient, is the shadow image of the focal spot formed around the image due to the fact that the focal spot has finite length and is not a point source (see Figure 2-18). The solid line represents the image formed by a point source. The dashed lines indicate the large edge that is formed by the finite-sized focal spot. A mathematical equation for the penumbra can be derived from the geometry in Figure 2-18. The penumbra is given by

$$P = \frac{C(A-B)}{B} \tag{2-25}$$

where A is the distance from the focal spot to the screen surface, C the effective size of the focal spot and B the distance from the focal spot to the object (in this case the collimator). The penumbra is therefore directly proportional to the focal spot size and screen distance, and inversely proportional to the object distance. The focal spot should be as small as possible to produce sharp images. The focal spot (target) is placed at an angle with respect to the screen, to enlarge the effective target area. This ensures that the target can be made large enough to take up all the heat produced during an exposure (see section 2.2, X-ray production), while the penumbra is kept small.

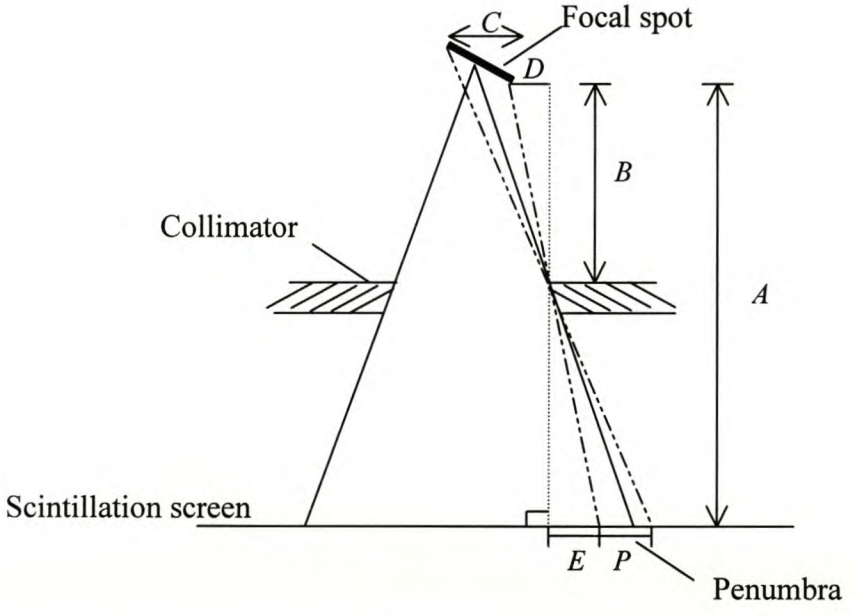

Figure 2-18: Graphical illustration of the geometric unsharpness in an image caused by the penumbra formed around an image.

Scattered X-rays are deflected in all directions, which only add noise to the imaging system and carry no useful information of the image. X-ray scattering inside the patient can not be eliminated, but is less for a high-energy X-ray beam than for a low energy beam. The scatter contribution to an image is less for longer set-up distances.

The resolution of a digital image is directly limited by the size of the matrix that represents the image. In screen film systems, the resolution is limited by the scintillation screen resolution,

which depends on the thickness, grain size and crystal structure (see section 2.4.5). The number of pixels on a CCD chip determines the spatial resolution that can be obtained with a digital imaging system. A higher number of smaller pixels will give a higher sampling frequency and therefore a higher resolution image, but with lower light sensitivity (see sampling, section 2.5.5).

The resolution of the image is expressed in line pairs per millimetre (lp/mm). The unit line pairs per millimetre can be thought of as viewing an image with a number of black lines separated by white spaces. As the frequency of the lines per unit length increases it becomes more difficult to distinguish between them, until they are so closely spaced that they can only be seen as a black homogeneous strip. The minimum interval size between lines that can be distinguished as separate lines (resolved) determines the limiting resolution. The limiting resolution is expressed as the highest frequency pattern in the image that can be resolved. Intuitively, because this is a frequency representation, it should be the reciprocal value of the minimum spacing between the two adjacent lines. It is important to remember that at least two pixels are necessary to resolve one line pair, one for the black line and one for the space between the line and the neighbouring line. The limiting frequency is therefore given by $\frac{1}{2\Delta x}$, where Δx is the minimum line spacing. This minimum frequency is again the Nyquist frequency (see sampling, section 2.5.5).

If it is known that the CCD chip limits the spatial resolution, the maximum obtainable resolution or system resolution is given by:

$$\text{System resolution (lp/mm)} = \frac{1}{2 \text{ x Effective pixel size}} \text{ (lp/mm)}. \qquad (2\text{-}26)$$

The effective pixel size is determined by the field of view (FOV), divided by the number of pixels on the CCD chip

$$\text{Effective pixel size} = \frac{\text{Field of view}}{\text{Number of pixels}} \qquad (2\text{-}27)$$

and the system resolution therefore becomes

$$\text{System resolution (lp/mm)} = \frac{\text{Number of pixels}}{2 \text{ x Field of view}} \text{ (lp/mm)} \qquad (2\text{-}28)$$

The system resolution is directly proportional to the number of pixels on the CCD chip and inversely proportional to the field of view.

The maximum resolution can also be defined in terms of the camera resolution, as specified by Edmund Scientific [Edm97]:

$$\text{System resolution (lp/mm)} = \text{PMAG x Camera resolution} \quad \text{(lp/mm)} \tag{2-29}$$

where PMAG is the primary magnification, defined by:

$$\text{PMAG} = \frac{\text{Sensor size}}{\text{Field of view}} \tag{2-30}$$

The camera resolution is given by

$$\text{Camera resolution (lp/mm)} = \frac{\text{Number of pixels}}{\text{2 x Sensor size}} \quad \text{(lp/mm)} \tag{2-31}$$

The system resolution (equation 2-28) again results from equations 2-29 to 2-31:

$$\text{System resolution (lp/mm)} = \frac{\text{Number of pixels}}{\text{2 x Field of view}} \quad \text{(lp/mm)}$$

The resolution of the imaging system can be determined with a test object that has a line pattern with lines spaced at known distances, or by calculating the modulation transfer function.

2.7.6 Measurement of spatial resolution: modulation transfer function

The modulation transfer function (MTF) is a mathematical function that expresses the ability of a system to transfer signals as a function of their spatial frequency. It is therefore used to measure the ability of an imaging system to reproduce an image of a specific object.

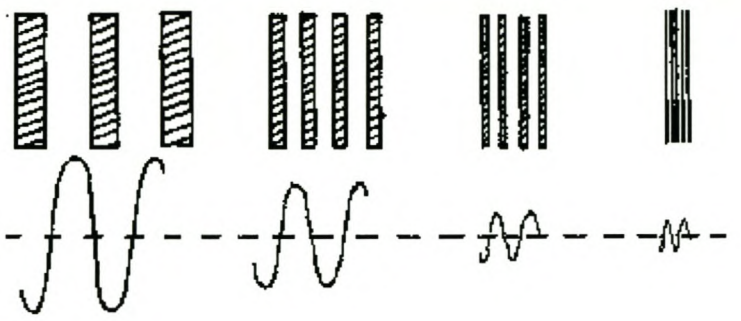

Figure 2-19: Illustration of the modulation transfer at different frequencies [Mer79].

The modulation of a signal is defined as the difference in minimum and maximum intensity values divided by their sum:

$$\text{Modulation} = \frac{I_{\max} - I_{\min}}{I_{\max} + I_{\min}} \tag{2-34}$$

where $I_{\max}$ is maximum intensity and $I_{\min}$ the minimum intensity in the signal (see Figure 2-20).

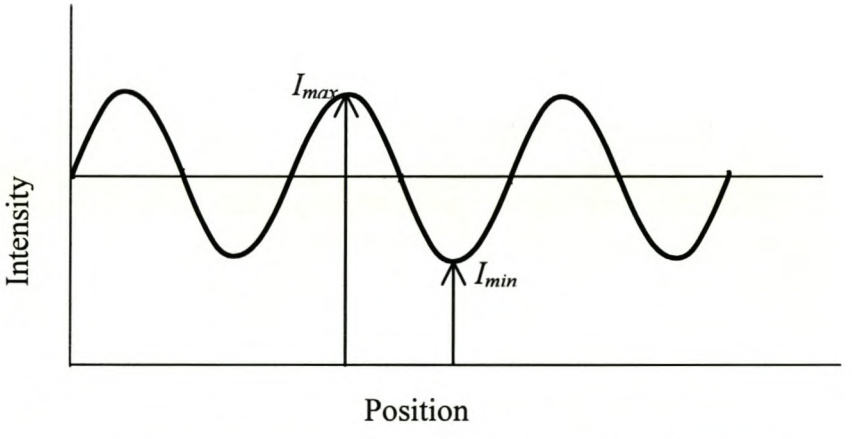

Figure 2-20: Intensity variation in an image signal.

Modulation transfer describes the amplitude modulation of the recorded signal relative to the amplitude modulation of the signal entering the system, over a range of frequencies.

$$\text{Modulation transfer} = \frac{\text{Output modulation}}{\text{Input modulation}} = \frac{M_o}{M_i} \tag{2-35}$$

The modulation transfer function is usually presented as a graph of $\frac{M_o}{M_i}$ plotted for different frequencies.

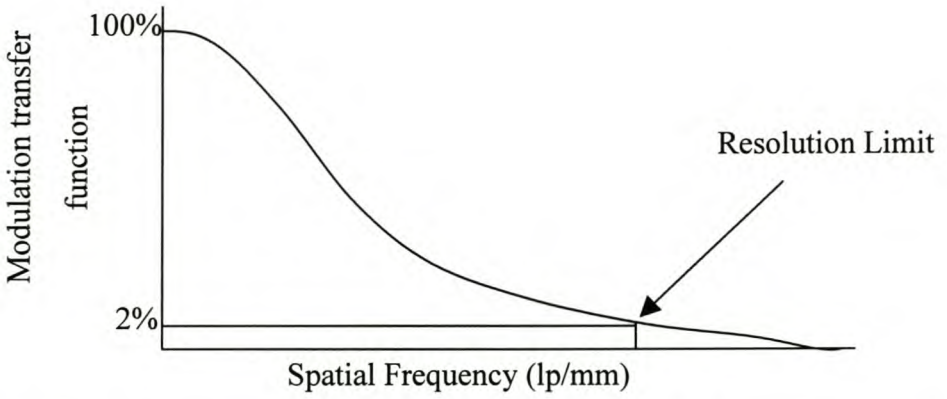

Figure 2-21: Modulation transfer function – the modulation of signals through the system, as a function of frequency.

The maximum obtainable resolution is read off at 2 % modulation transfer, since the contrast between structures imaged with modulation transfer smaller than 2 % is too small to resolve. The Rayleigh criterion for resolution of fine structures in an image specifies the maximum spatial resolution as the value read off at 10 % intensity modulation on the *x*-axis (MTF = 0.10) [Hal93]. The shape of the MTF at lower frequencies gives an indication of the image sharpness. If the MTF drops rapidly, the image is not sharply focussed, even though the high frequency structures are resolved, in the same way as the gradient of the edge spread function indicates the resolution while the long tail represents the unsharpness [Bra98]. The frequency scale on the *x*-axis is determined by the theoretical maximum resolution with increments according to the number of points used for obtaining the Fourier transform.

The MTF can be obtained from the Fourier transform (Fast Fourier Transform algorithm (FFT)) of the line-spread function (LSF), as described below and illustrated in Figure 2-21 and Figure 2-22. The Fourier transform of the line-spread function (LSF) is called the optical transfer function (OTF) [Fuj85]. The LSF is determined from the cross section through a narrow slit image, or the derivative of a cross section through a step-function image or edge spread function (ESF) [Fis81]. The optical transfer function is a complex function with amplitude (or modulus) and phase components, called the modulation transfer function (MTF) and the phase transfer function (PTF) respectively.

The OTF can be split into different parts, describing the influence of the different components on the resolution of the system separately. The OTF can further be written as a product of the pre-sampling or analog OTF and the digital OTF. The factors influencing the pre-sampling OTF are the geometric unsharpness, the detection system and the optical system. The digital OTF measures the contribution of digitisation. Important factors contributing to the digital OTF are the sampling rate, sampling aperture (which is equal to the sampling rate for square pixels), and quantisation levels (see quantisation, section 2.5.5). It has been explained that the quantisation effect is negligible for a 16-bit ADC converter.

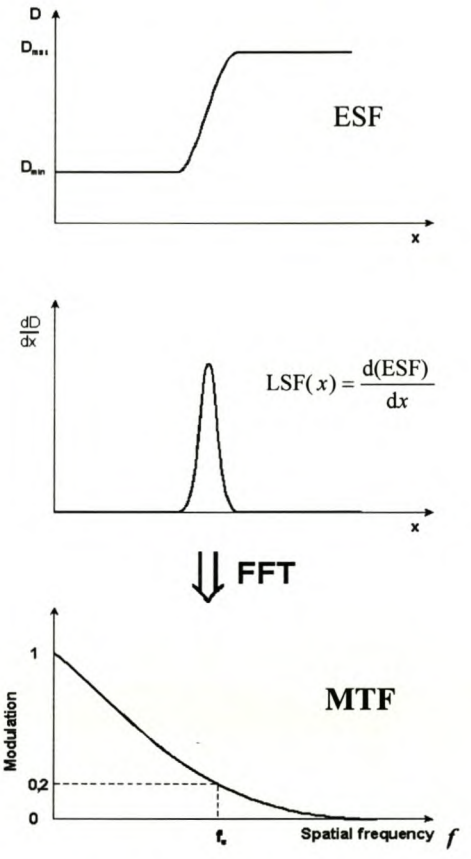

Figure 2-22: Measurement of the modulation transfer function. The edge spread function (ESF) gives the intensity difference around a sharp edge; the derivative of the ESF gives the line spread function and the modulus of the Fourier transform shows the modulation transfer as a function of frequency.

2.7.7 Gibbs effect (FOV smaller than object)

If the FOV is smaller than the object the edges of the image are cut off sharply and will be discontinuous. These boundary discontinuities cause additional high frequency components to be added to the image when the Fourier transform is taken. This is known as the Gibbs effect, which can be seen as ringing in the image when the inverse Fourier transform is taken, because of high frequency components added to the image. The high frequency components are added by the sharp edge, since many high frequency components are needed to reconstruct a sharp edge, just as low frequency components in the Fourier domain characterises uniformity in an image. The mathematical explanation of the Gibbs effect is that the Fourier transform does not converge uniformly at discontinuities and takes on mean values at the points of discontinuity [Gon93].

Using the discrete cosine transform (DCT) instead of the Fourier transform can eliminate the Gibbs effect. In the discrete cosine transform the image is extended periodically in such a way that the image is reflected at its edges so that there are no discontinuities [Gon93]. The Gibbs effect can be reduced by increasing the field of view (FOV), filtering the image with a low pass filter to remove the additional high frequency components added to the image or increasing the sampling frequency (Nyquist limit) by increasing the matrix size (resolution).

The CCD chip pixel size determines the sampling frequency, i.e. the Nyquist frequency (see section 2.5.5 – the effect of sampling on an image). With a sampling frequency F_s, the highest frequency that can be reconstructed uniquely (according to the sampling theorem, Appendix A) is $F_s/2$.

Aliasing occurs when a signal is sampled at a rate lower than required by the sampling theorem. Frequency components in the signal with higher frequencies than the Nyquist frequency can be falsely represented as lower frequencies. This can be explained by looking at a sinusoidal signal. For a continuous sinusoidal signal, represented by

$$f(x) = A \cos(2\pi F_0 x + \phi), \tag{2-36}$$

with F_0 the fundamental frequency. The corresponding sampled signal is

$$f(n) = A \cos(2\pi f_0 n + \phi). \tag{2-37}$$

where f_0 is the digital frequency and n the sampling intervals.

Two analog signals with different frequencies can be represented by one digital signal if the frequency of one signal is an integral multiple of the other. A signal with frequency higher than $F_s/2$ will be represented incorrectly as a signal with a lower frequency, equal to an integer multiple of the frequency of the original signal. This lower frequency signal is referred to as an alias of the original signal and the phenomenon is called aliasing.

The influence of the analog components in the imaging system on the spatial resolution can be determined by measuring the pre-sampling MTF [Nei94]. The pre-sampling MTF is obtained by using a slightly angulated slit to obtain a highly sampled line spread function and eliminating the affect of aliasing introduced by the sampling rate of the CCD chip [Fuj92]. If the CCD chip resolution is increased, the pre-sampling MTF can be used to determine which analog component limits the system resolution.

2.8 Digital images

2.8.1 Image Processing

Read-out noise and quantisation noise contributions are inherent to the CCD chip and analog to digital converter of the CCD camera and can not be removed by the user. By reducing the read-out rate the read-out noise can be decreased [Koc94], but the read-out time is normally fixed.

The bias signal and thermal noise can be removed from the image by subtraction of a dark current exposure. A dark current image is obtained by taking the average of a number of dark current images with exposure time the same as for the CCD image but without opening the shutter of the camera. This will give the bias signal together with only the thermal noise contribution, because no photons will fall onto the CCD chip. The thermal noise can be reduced significantly by cooling the CCD chip.

There are numerous image enhancement techniques available, from sharpening filters to noise reduction filters [Gon93]. A thorough discussion of image processing techniques falls outside the scope of this thesis.

Photon noise, beam inhomogeneities and efficiency variations across the CCD chip can be corrected by flat fielding, as explained below.

A flat field image is an image illuminated by a uniform source, i.e. an image of an X-ray exposure with no object. Each value of the dark current corrected CCD image is divided by the values of the normalised flat field image to remove sensitivity variations in the detection system and to correct for the shape of the X-ray beam. If I'_{ij} is the raw image value at position (i,j), D_{ij} the corresponding dark current image value and F_{ij} the flat field image value, then the processed image is given by [Boy92]:

$$I_{ij} = \frac{I'_{ij} - D_{ij}}{F_{ij} - D_{ij}} \tag{2-38}$$

2.8.2 Image display

The digital images are displayed on a PC monitor; a high contrast monitor could be used to obtain higher visual contrast. The advantage of the digital system over film is that the display contrast on the screen can be varied, whereas film has a characteristic curve with a fixed slope and the image contrast can not be changed. A logarithmic function of the greyscale image values is displayed to compensate for exponential attenuation in the patient [Alt96].

2.8.3 Image file formats

The digital image file format refers to the structure of data stored in an electronic file. There are several image file format standards available according to the requirements of the particular application. The two basic types of image formats are raster formats, consisting of an array of pixels each containing a colour value, and vector formats, in which an image is described in terms of a group of mathematically defined shapes with colours and other attributes associated with the shape. Windows Bitmap (BMP), created by Microsoft, OS/2 Bitmap (OS/2 BMP) created on an OS/2 operating system and the tag-based file format TIFF (Tagged Image File Format) are the most commonly used raster formats. Microsoft bitmap images have headers containing fixed fields such as the width and height of the grid followed by the image data. The power of bitmap images relies on the use of indexing, where a fixed or customisable palette is added to the image and each of the colour values for each pixel is represented by a palette index.

Bitmap therefore offers fast and effective screen display. The TIFF file header has a structured heading containing the necessary information about the type and position of the image data, which can be placed anywhere in the file. TIFF is therefore a flexible image file format, which can be used for saving multiple images into one file, is not restricted to a specific data structure and can easily handle large files.

The file format well known for its compression capability is JPEG, developed by the Joint Photographic Experts Group. Compression algorithms are used to decrease the overall file size by grouping same-coloured pixels, averaging colour transitions, coding (see section 2.5.5) and various other methods. The compression can either be lossy, where image information is lost, or lossless where all of the detail of the original image is retained. Lossy algorithms achieve greater compression by averaging out differences, taking advantage of the limitations of the human eye, but can not be used for radiographic images where image detail is of absolute importance.

DICOM (Digital Imaging and Communications in Medicine) is a file transfer protocol mainly used as a file format for medical imaging applications [ACR93]. The DICOM file type provides the most complete support of colour spaces and compression types and also facilitates the handling of multiple images, such as the frames of a cine loop, in a single file.

2.9 Dose calculations

X-rays are ionising radiation and cause biological damage to the patient. The degree of biological damage is determined by the amount of radiation, the radiation quality and the sensitivity of individual human organs to the type of radiation. The amount of energy deposited in a material by ionising radiation per unit mass is defined as the absorbed dose. The units of absorbed dose is gray (Gy), which is equal to one joule per kilogram (J/kg), and 1 gray (1 Gy = 1 J/kg) equals 100 rad [Joh83]. The radiation quality is specified for each radiation type to evaluate the biological damage caused by the specific radiation. The effect of an amount of radiation on a specific organ is also taken into account, since different organs are not equally sensitive to ionising radiation. However, the determination of the biological damage caused by radiation is quite complicated. The surface entrance dose is therefore measured as a reference dose to give a relation of different radiation doses [Mar99].

It is possible to determine the absorbed dose indirectly by measuring the exposure in roentgen, R, since the exposure also represents the amount of energy absorbed from the beam irrespective of the radiation quality, but specifically in air [Mer79]. The exposure, which specifies the amount of energy absorbed per unit mass in air, is converted to absorbed energy in a material by the mass absorption coefficient [Mer79]. The energy absorbed per unit mass from an exposure of 1 roentgen (1R) in air corresponds to an absorbed dose of 8.69 mGy.

The absorbed energy per mass is equal to the energy in the beam multiplied by the mass absorption coefficient [Mer79].

$$\text{Absorbed energy per mass} = E\left(\frac{\mu_a}{\rho}\right) \tag{2-39}$$

The ratio of the absorbed energy per mass of the material to the absorbed energy in air is therefore given by

$$\frac{\text{Absorbed energy per mass (material)}}{\text{Absorbed energy per mass of air}} = \frac{E\left(\frac{\mu_a}{\rho}\right)_{Material}}{E\left(\frac{\mu_a}{\rho}\right)_{air}} \tag{2-40}$$

If the energy absorbed per unit mass in air is equal to 0.869 R, the energy absorbed in the material per unit mass is:

$$\text{Absorbed energy per mass (material)} = \frac{8.69\,D\left(\frac{\mu_a}{\rho}\right)_{Material}}{\left(\frac{\mu_a}{\rho}\right)_{air}} \text{ mGy} \tag{2-41}$$

$$= f \quad D \quad mGy \tag{2-42}$$

with f in equation 2-42 the roentgen to gray conversion factor given by 8.69, multiplied by the ratio of the mass absorption coefficients of the material and air and D the measured exposure. The mass absorption coefficients, and therefore the values of f, are known for most materials and are given for water, muscle and bone for different radiation energies [Mer79].

Chapter 3

Materials and methods

3.1 Introduction

Different set-up configurations and components were investigated and compared to provide guidelines for solving the problems involved in constructing a digital imaging system similar to the one described in this thesis. Several factors concerning the imaging set-up, performance of individual components as well as the total system performance were considered.

The digital imaging system consists of a scintillator screen, a front silvered mirror, and a charge coupled device (CCD) camera, placed in a light tight cover (see Figure 3-1). The images are displayed on a personal computer. The scintillator screen converts X-ray photons to visible light photons in the sensitive range of the CCD camera. The front silvered mirror reflects the light to the camera, which is placed out of the X-ray beam to avoid damage to the electronic components. The lens focuses the light onto the CCD chip, which captures the image and converts it into digital format.

The overall performance of the imaging system is evaluated in terms of its spatial resolution, the light yield, the system noise and the dose given to a patient from the X-ray exposure. The individual components were chosen to optimise the overall performance of the imaging system.

3.2 Digital imaging system set-up

The X-ray image is an intensity distribution resulting from the difference in attenuation in the various parts in the patient. The X-ray image is converted to a two dimensional light image in the scintillator screen, which is a projection of the X-ray image according to the number of X-ray photons falling onto the screen. The light image from the screen is reflected to the camera by a front silvered mirror. A front silvered mirror is used to ensure that light is reflected from the first surface alone and not from the back of the mirror. Multiple reflections, for example from the front and back of a mirror, reduce the image resolution and therefore the quality of the image.

The mirror is positioned 80 millimetres from the nearest corner of the scintillation screen, at a 45° angle. The separation between the screen and the mirror is necessary to reduce the contribution of scattered light from the mirror back to the screen and again to the mirror [Bo98b], [Koc94]. The light image from the mirror is collected by the lens and focussed onto the CCD chip. The camera is placed 450 mm from the mirror. The focal length of the lens is 11 mm and the scintillation screen size (field of view) 200 x 300 mm^2. The components are placed inside a light tight cover. The image is collected onto the array of CCD pixels, digitised, read out and displayed on a personal computer.

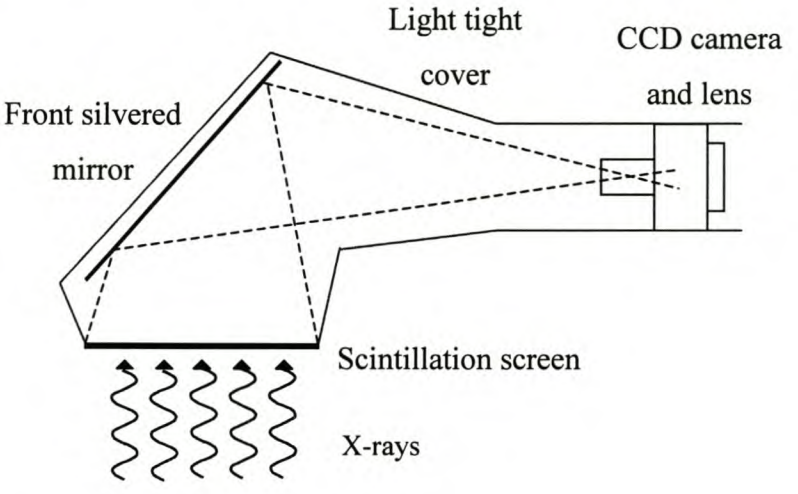

Figure 3-1: The digital imaging system consists of a scintillation screen, a front silvered mirror and a CCD camera.

3.3 Imaging components

3.3.1 Scintillation screens

Different scintillation screens were compared in terms of the light yield and resolution. The scintillators that were used are Gd_2O_2S:Tb (Rarex), ZnCdS:Ag (PFG) from MCI Optonix [Mci99] and the traditional calcium tungstate ($CaWO_4$) screen (Dupont Cronex Hi-Plus). Two Rarex screens with different thicknesses and deposition densities of Gd_2O_2S:Tb were used. The Gd_2O_2S:Tb screens are labelled Rarex G-130 and Rarex G-50 with deposition densities of 130 mg/cm^2 and 50 mg/cm^2 respectively. The phosphor material is deposited onto a plastic support backing and is covered by a 10-12 μm protective coating. The measured thickness of Rarex G-130 was 0.57 mm and Rarex G-50, 0.42 mm (screen and plastic support/backing). The

plastic support for the screens is 0.0267 mm [Mci99] and the phosphor thicknesses for Rarex G-130 and G-50 are therefore 0.54 mm and 0.39 mm respectively (see Table 3-1, [Ryn95]). The thickness of the calcium tungstate screen and backing is 0.47 mm. The Rarex G-130 and G-50 screens have visual resolution (screen resolutions) of 5.0 and 6.3 line pairs per millimetre respectively and the PFG screen 2.5 line pairs per millimetre. Additional specifications for the screens are given in Table 3-1.

Table 3-1: Scintillation screen properties [Ryn95], [Mci99].

Scintillation Screen	Composition	Emission efficiency	Deposition density (mg/cm^2)	Phosphor thickness (mm)	Visual screen resolution (lp/mm)	Wavelength peak (nm)
Calcium Tungstate	$CaWO_4$	5 %	142.1*	-	< 2.5	425
LANEX	Gd_2O_2S:Tb	18 %	-	0.38	< 5.0	545
Rarex Green Fine	Gd_2O_2S:Tb	16 %	-	0.34	-	545
Rarex Green Fast G130	Gd_2O_2S:Tb	16 %	129.2	0.53	5.0	545
Rarex Green Regular G50	Gd_2O_2S:Tb	16 %	57.8	0.39	6.3	545
Rarex PFG	ZnCdS:Ag	19 %	119.2	0.63	2.5	530

*Value measured for Dupont Cronex Hi-Plus calcium tungstate screen

The line spectrum of Gd_2O_2S:Tb is shown in Figure 3-2. Calcium tungstate ($CaWO_4$) has a broad emission spectrum with an intensity peak at 430 nm [Cur90], [Joh83]. The emission spectrum of ZnCdS:Ag is also a broad emission spectrum peaked at 530 nm [Joh83].

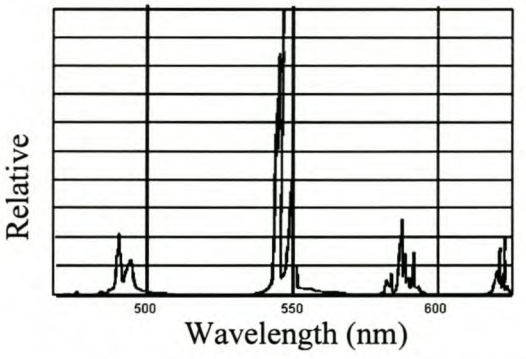

Figure 3-2: Emission spectrum (line spectrum) of Gd_2O_2S:Tb with emission peak at 545 nm. (From Applied Scintillation Technologies [Appst99]).

3.3.2 CCD camera

The CCD camera (Hi-SIS22, Lambert Instruments, the Netherlands) contains a Kodak KAF-0400 CCD chip. The CCD chip consists of an array of 512 x 768 CCD elements or pixels of size 9 x 9 μm^2 onto which the image is collected and stored. After charge collection, the image is transferred to an output node on the CCD chip and digitised by a 16-bit analog to digital converter on the chip. The images are saved as 16-bit TIFF images by the camera software Hi-SIS, also from Lambert Instruments. The digitised image can be processed and displayed on computer.

The CCD chip is not equally sensitive to all wavelengths of light. The spectral response of the CCD chip indicates the sensitivity or quantum efficiency of the chip to different wavelengths. The spectral response for the Kodak KAF-0400 CCD chip is given in Figure 3-3. The relatively high emission wavelength peak of Gd_2O_2S:Tb at 545 nm matches well with the high quantum efficiency of the CCD chip at this wavelength.

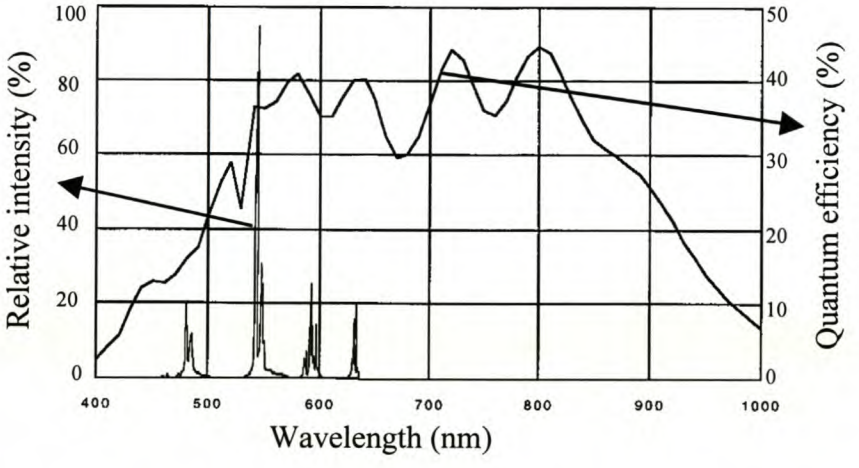

Figure 3-3: The emission spectrum of Gd_2O_2S:Tb superimposed on the graph of the quantum efficiency of the Kodak-0400 CCD chip.

Keeping the CCD chip temperature low, using thermoelectric (Peltier) cooling, reduces thermal or dark current noise added to an image during charge accumulation. The dark current is sufficiently reduced from 11 electrons per pixel per second without cooling to 0.04 electrons per pixel per second. The full well capacity of the CCD chip is 7.9 x 10^5 electrons per pixel. (CCD chip sensitivity = 1.5 x 10^6 electrons per pixel per lux per second [Lam99]). The dynamic range

for the KAF-0400 is > 72 dB [Lam99]. The electronic offset or bias signal of the CCD chip is between 1800 and 1820 ADU (analog to digital conversion unit). An ADU corresponds to 2.4 electrons per pixel, as tested for our camera [Lam99]. The read-out noise is less than 9 ADU, in other words 22 electrons per pixel [Lam99]. The digitisation error is negligibly small for 16-bit images. The minimum shutter speed of the camera is 0.005 – 0.01 seconds (CCD specifications [Lam99]).

3.4 Focussing the camera

The read-out time of a full-scale image at full resolution is less than 4 seconds [Lam99]. This is a very short interval, but causes dead time between successive images, which makes focussing very difficult. For focussing purposes, the acquisition and read-out time can be sufficiently reduced by using short exposures and pixel binning. If two adjacent pixel values are added together in both the horizontal and vertical directions (2 x 2 binning) the read-out time is reduced by a factor of four. However, the resolution is halved in each direction and therefore binning is only used to focus the camera initially.

Visual focussing of full resolution images is not only time consuming, but also inaccurate, as it is difficult to compare the image sharpness of two images taken a few seconds apart. For this reason the image sharpness is determined analytically by comparing the slope of the edge spread function of the subsequent images. If the field of view is unchanged, the number of pixels with values in the edge spread function gives an indication of the image sharpness [Bar98]. A sharply focussed image has a very steep gradient compared to an unfocussed image [Mer79]. The edge-spread function of an unfocussed image is therefore stretched out and more pixels or image values will be represented in the curve. This is only true for a fixed field of view, with the object size projected onto the chip kept the same and the pixel intervals unchanged. The number of pixels in the region between 20% and 80% of the intensity of the edge spread function is used as a reference to measure the image sharpness [Bar98].

3.5 Physical set-up

In the final application of the system, two X-ray images are superimposed onto each other. The first image is an open field image of the patient containing anatomy information [Hou99]. The second is taken through the collimator that traces the outline of the collimator with respect to the

anatomy. In the current system, the images are recorded by taking a double exposure onto a single film. The digital images obtained with the new system will be combined into one image by adding corresponding image values (matrix addition). For the open field image, the scintillation screen is placed 1100 millimetres from the focal spot of the X-ray tube. The image with the collimator is taken with the X-ray tube placed further away from the screen at 2 000 mm and the collimator 530 mm from the screen. The patient is positioned 300 mm from the screen to reduce the contribution of scattered radiation from the patient to the image. The light image is focussed onto the CCD chip by a zoom lens with focal length 11 mm and an aperture of *f*/1.0, to obtain a high light yield. The CCD camera is placed 450 mm from the centre of the mirror to obtain a field of view of 200 x 300 mm^2.

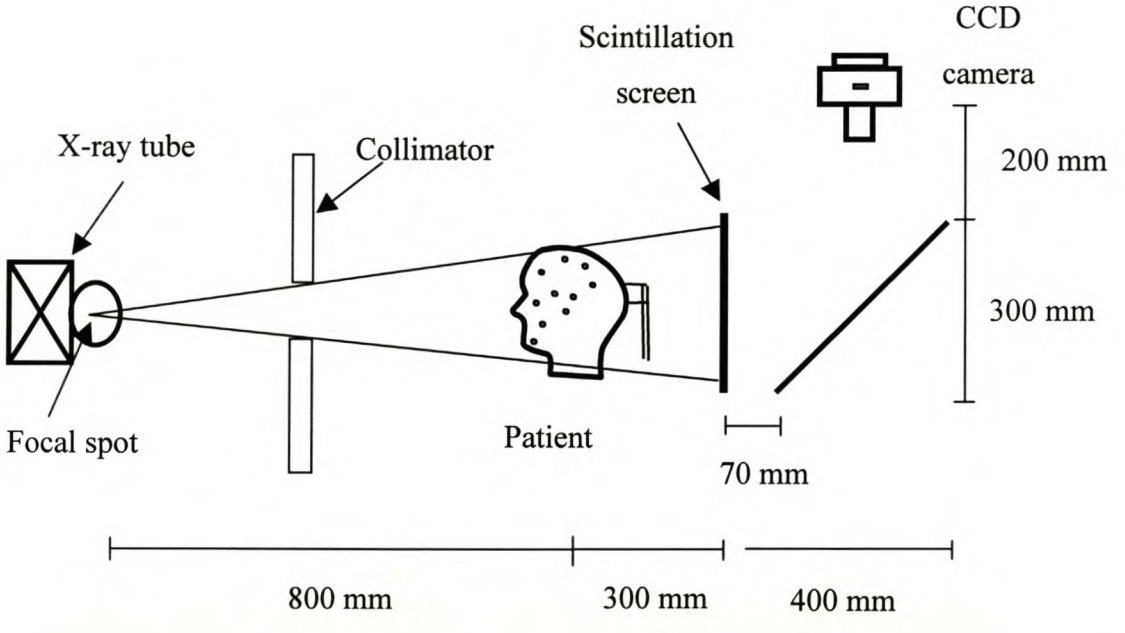

Figure 3-4: Diagram of the physical arrangement of the X-ray tube, patient and digital imaging system, for an open field image set-up.

3.6 Camera shielding

The camera is positioned outside the X-ray beam to avoid damage to electronic circuits from direct X-rays. Additional shielding is placed between the camera and the X-ray tube to absorb scattered X-ray photons. A 2 mm thick lead shield is used and this is sufficient to stop 99 % of a 120 kVp X-ray beam.

3.7 System performance

3.7.1 Light yield

The relative light yield of the digital system was measured for Rarex G-130, Rarex G-50, PFG and calcium tungstate screens, with exposures of 80 kVp and 20 mAs. The image values are given in terms of analog to digital conversion units (ADUs), see section 3.3.2. Figure 3-5 and Figure 3-6 illustrate the light yield measurement for the Rarex G-50 and Rarex G-130 scintillation screens, obtained with a single exposure. The screens were mounted onto one mounting next to each other (see Figure 3-5). This was done to compare the light yield from a single exposure and to eliminate any uncertainties in the number of X-ray photons from separate exposures.

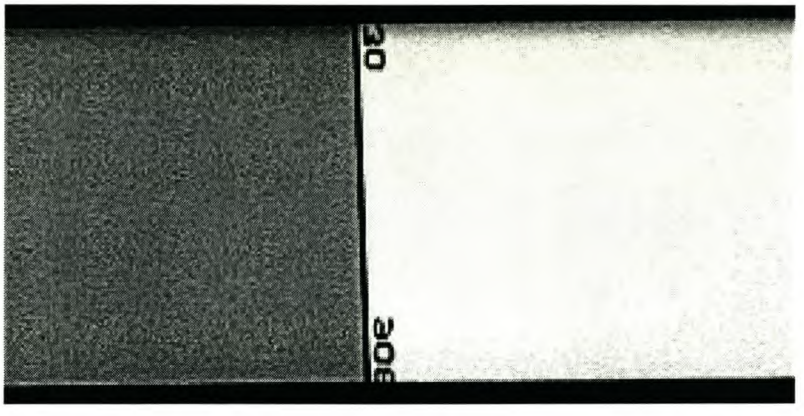

Figure 3-5: Digital light image of Rarex G-50 (left) and Rarex G-130 (right) scintillation screens obtained with a single X-ray exposure.

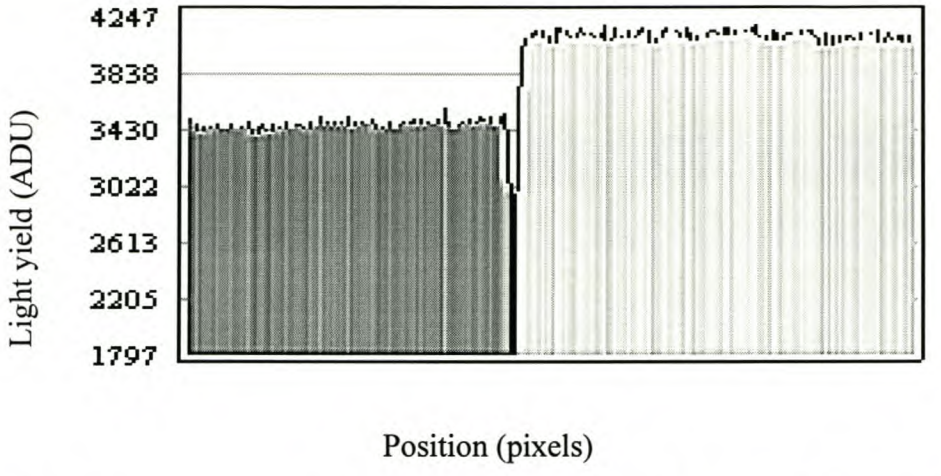

Figure 3-6: Cross section through the Rarex G-50 and Rarex G-130 screens, shown in Figure 3-5, to illustrate the relative light yield measured in ADUs.

The influence of the screen backing was investigated by comparing the light yield obtained from a single exposure using one scintillating screen with different mounting segments. The light yield obtained with the Rarex G-130 screen was determined using small pieces of aluminium of different thicknesses and a perspex plate, joined to form a mounting for the scintillator screen. Aluminium thicknesses of 1.5 and 1.1 mm and a 1.5 mm perspex backing were used, with exposures of 60 to 80 kVp.

3.7.2 Spatial resolution

The spatial resolution was determined by taking X-ray images of a test object and measuring the modulation transfer function. The test object that was used is a wire phantom consisting of four groups of copper wires with spacings 1.25 mm, 0.83 mm, 0.63 mm and 0.50 mm, corresponding to 0.8, 1.2, 1.6 and 2.0 line pairs per millimetre respectively. Two different CCD camera fields of view of 290 x 190 mm and 160 x 110 mm were used. The test object was placed close to the scintillation screen and X-ray images were obtained with exposures of 60 kVp and 20 mAs.

The modulation transfer function for our system was measured by taking the Fourier transform of the derivative of the edge-spread function [Fis81]. The edge-spread function is a cross section through an X-ray image of a sharp metal edge, indicating the drop from high to low X-ray intensity. A 10 mm thick copper plate is placed tightly against the scintillation screen to

obtain the sharpest possible gradient, i.e. by avoiding the contribution of scattered rays from the divergent X-ray beam. The influence of the focal spot size and possible magnification on the image are also eliminated when the test object is placed in contact with the screen [Fis81], [Mu90b], [Dro85], [Mer79]. Exposures of 80 kVp and 20 mAs were used.

For a field of view of 300 x 200 mm^2, the effective pixel size, in one dimension, is

$$\text{Effective Pixel Size}\,[\text{mm}] = \frac{300}{768}\ \ [\text{mm}] \tag{3-1}$$

and the theoretical (Nyquist) limit for the system resolution is

$$\text{System resolution}\,[\text{lp/mm}] = \frac{768}{2 \times 300} = 1.28\ \ \ [\text{lp/mm}]\,. \tag{3-2}$$

The resolution limit can also be defined in terms of the primary magnification (PMAG), given by the sensor size divided by the field of view, and the camera resolution (equation 2-29):

$$\text{System resolution (lp/mm)} = \text{PMAG x Camera resolution(lp/mm)} \tag{3-3}$$

$$\text{Camera resolution (lp/mm)} = \frac{\text{Number of pixels}}{\text{2 x Sensor size}}\ \ (\text{lp/mm}) = \frac{768}{2 \times 6.4} = 60\ \ \text{lp/mm} \tag{3-4}$$

The primary magnification factor (equation 2-30) is:

$$\text{PMAG} = \frac{\text{Sensor size (H)}}{\text{FOV}} = \frac{6.4\,\text{mm}}{300\,\text{mm}} = 0.0213. \tag{3-5}$$

$$\begin{aligned} \text{System resolution (lp/mm)} &= \text{PMAG} \times \text{Camera Resolution (lp/mm)} \\ &= 0.0213 \times 60\ \ \text{lp/mm} \\ &= 1.28\ \ \text{lp/mm} \end{aligned} \tag{3-6}$$

This is the maximum obtainable resolution with a field of view (FOV) of 300 x 200 mm^2. Since the maximum obtainable image resolution depends on the pixel size it is possible to improve the resolution by decreasing the field of view. Using a lens with a longer focal length and a shorter

minimum focal distance can decrease the field of view. For a field of view of 160 x 110 mm^2 the Nyquist resolution limit for the system resolution is 2.4 lp/mm.

3.7.3 Image quality

The influence of the light scatter between mirror and scintillator on the image quality was investigated. Anterior posterior (AP) X-ray images were taken of a skull phantom (human skull imbedded in tissue equivalent perspex) with different spacings between the mirror and the scintillation screen. The part of the mirror closest to the scintillation screen was covered to produce the effect of a larger spacing between the screen and mirror, in odder to reduce scattering in the image. In the first arrangement an image is obtained with 70 mm of the mirror covered. This image is compared with an image taken with the mirror placed directly next to the screen. The X-ray images were taken with exposures of 90 kVp and 20 mAs with the same field of view and scintillation screen to CCD camera distances. The image quality and resolution for different set-up positions were compared.

The effect of vignetting and the reduction of image quality at the edges were investigated by using different lens focal lengths of 8 mm and 10 mm. The camera is moved further away from the scintillation screen when using a 10 mm lens to maintain the same field of view and also to focus the image, since the minimum focus distance of the lens is longer for larger focal lengths.

3.7.4 Dose measurement

The absorbed dose given to a patient from a single X-ray exposure was measured. Our aim is to produce high quality digital X-ray images while reducing the exposure from that currently given when using radiographic films.

The absorbed dose was measured for different exposures. The quality of the images obtained with the different exposures was also compared. The dose was measured at the source to isocentre distance (SID), 350 mm from the screen, using an ionisation chamber. The measured value was converted to a value at screen entrance, referred to as the source fluorescent screen distance (SFD). The conversion from dose value at the SID (D_{SID}) to the dose at the screen entrance (D_{SFD}) was calculated using the inverse square law: $D_{SFD} = D_{SID} \times (SID/SFD)^2$. The distance from the source or focal spot to the isocentre (SID) was 875 mm and the source to

screen distance (SFD) 1250 mm. The ionisation chamber is calibrated in Roentgen and the exposure is converted to absorbed dose using the conversion factor $f = 0.01$ mGy/Roentgen for X-ray beam energy 100 keV [Mer79].

Chapter 4

Results and discussion

4.1 Introduction

Experiments were performed to measure the light yield and resolution for the system with different scintillation screens. The effect of the screen mounting on the light yield was also tested and the influence of scattered light on the resolution was investigated for different set-up configurations.

4.2 Light yield

The same light yield was measured with the PFG and the Rarex G-130 screens using the digital system. PFG (ZnCdS:Ag) has an emission efficiency of 19 % and Rarex only 16 %. Furthermore, the thickness of the phosphor layer of Rarex G-130 was also less than that of the PFG screen (see Table 3-1 in Chapter 3). The deposition density (in mg/cm^2) of Rarex G-130 was slightly higher than for PFG. The measured light yield values are given in Table 4-1. The fact that similar light yields are obtained with the two screens is assigned to better matching with the CCD chip at the emission wavelength of Rarex G-130 (545 nm) than for PFG which has a lower emission wavelength peak (530 nm) and also partly because of the higher deposition density of Gd_2O_2S:Tb. The lower emission efficiency and deposition density of the Rarex screen are compensated for by the higher quantum efficiency of the CCD chip at wavelengths higher than 545 nm (see section 3.3.2 – the spectral response of the CCD chip). The light yield measured for Rarex G-50 is lower than for Rarex G-130 as expected because of the lower deposition density of G-50. The calcium tungstate screen has a high deposition density but produced a low light yield due to the low emission efficiency and short emission wavelength (close to the ultra violet range), causing unfavourable wavelength matching with the CCD chip.

Table 4-1: Relative light yield measured with different scintillator screens, normalised to Rarex G-130

Scintillation screen	Scintillator material	Emission efficiency	Emission wavelength (nm)	Measured light yield (relative)
Rarex G-130	Gd_2O_2S:Tb	16%	545	100 %
Rarex G-50	Gd_2O_2S:Tb	16%	545	76 %
PFG	ZnCdS:Ag	19%	530	98 %
Calcium Tungstate	$CaWO_4$	5%	425	30 %

The light yield obtained with different thicknesses of aluminium and plastic backings from a single exposure of the Rarex G-130 scintillating screen was compared. The light yield obtained with the 1.5 mm aluminium backing was lower than for the 1.1 mm aluminium backing. The aluminium backings caused a considerable amount of attenuation of the X-ray beam in comparison with the plastic mounting. A higher light yield was obtained using the 1.5 mm plastic mounting. The light yield measured with the plastic mounting was nearly the same as obtained with the scintillator screen alone, which indicates that there is minimal X-ray attenuation in the plastic. The plastic backing will therefore be used to support the scintillation screen.

4.3 Spatial Resolution

The images of the wire phantom are shown in Figure 4-1 below. The first image is obtained with a field of view of 290 x 190 mm^2 and the second with a smaller field of view of 160 x 110 mm^2. By zooming in, i.e. reducing the field of view it was possible to increase the image resolution (see section 2.7.5 – spatial resolution). The first two quadrants of the wire phantom are resolved in the first image and the third is nearly resolved, indicating that the maximum obtainable resolution is just below 1.6 line pairs per millimetre. The theoretical (Nyquist) limit for a field of view of 290 x 190 mm^2 is 1.32 lp/mm. In the second image, all four quadrants are resolved and the resolution is therefore 2 line pairs per millimetre or more. The Nyquist limit for this field of view (160 x 110 mm^2) is 2.4 lp/mm.

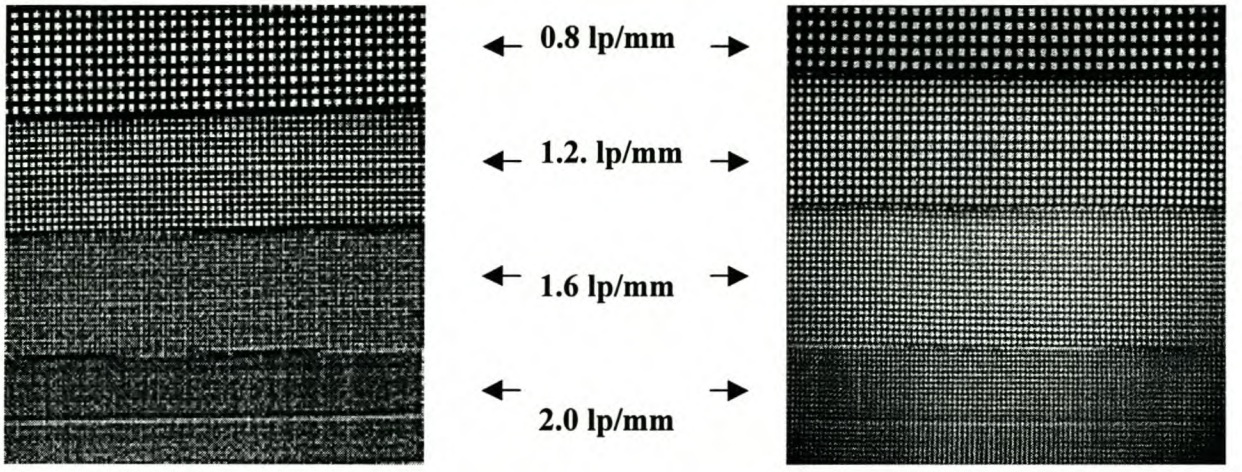

Figure 4-1: Images of a wire phantom. The left-hand side image is taken with a field of view of 290 x 190 mm^2 and the right-hand side image with a field of view of 160 x 110 mm^2.

The edge-spread functions of the various scintillation screens that were tested are given in Figures 4-2 (a) and (b). The field of view for the measurement of the spatial resolution with the Rarex screens was 290 x 190 mm^2 and for the PFG and $CaWO_4$ screens, 300 x 200 mm^2. Figures 4-3 (a) and (b) show the modulation transfer functions obtained from the measurement of the edge spread functions shown in Figure 4-2.

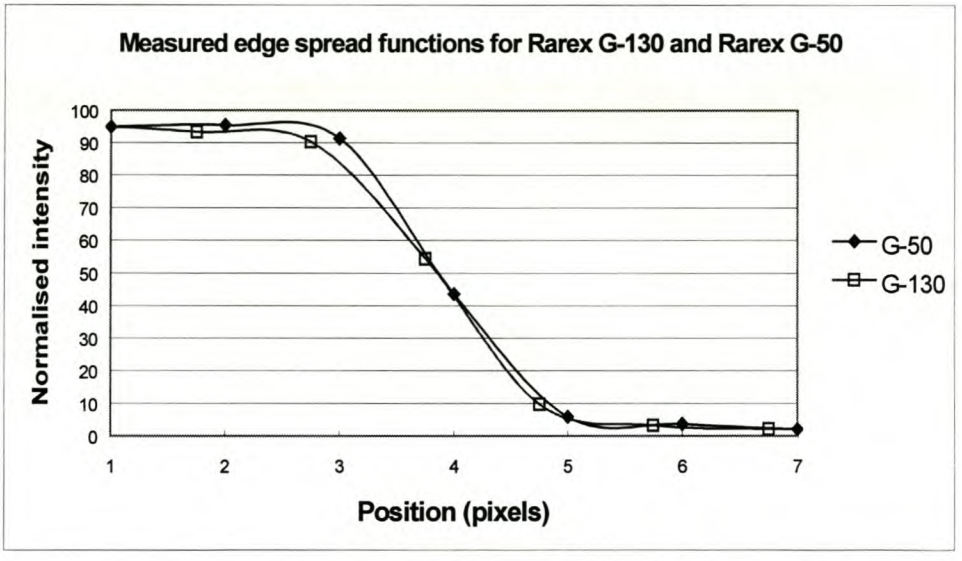

Figure 4-2 (a): Measured edge spread functions for Rarex G-50, Rarex G-130, measured with a field of view of 290 x 110 mm^2.

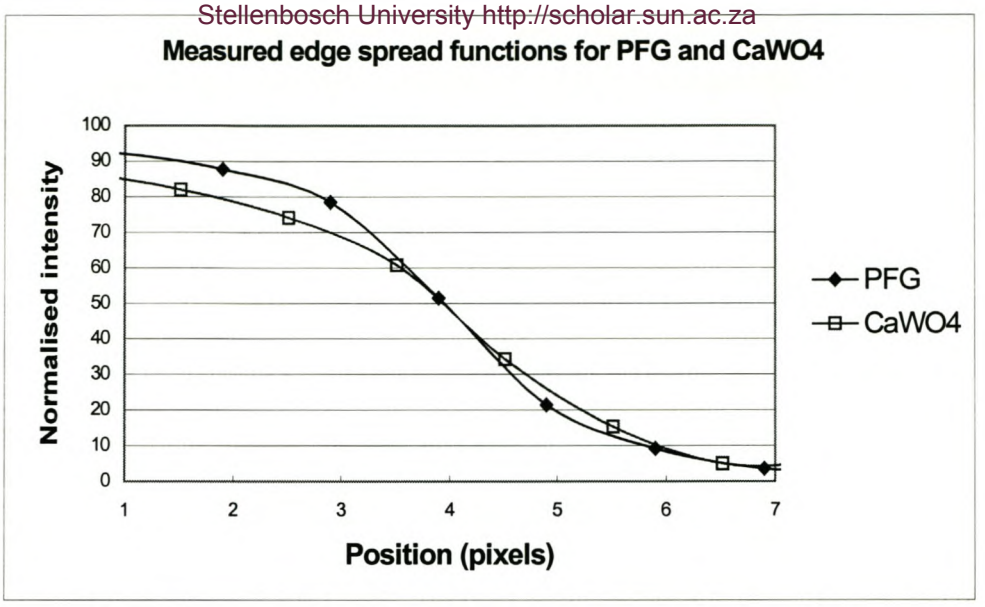

Figure 4-2 (b): Measured edge spread functions for PFG and $CaWO_4$, measured with a field of view of 300 x 200 mm^2.

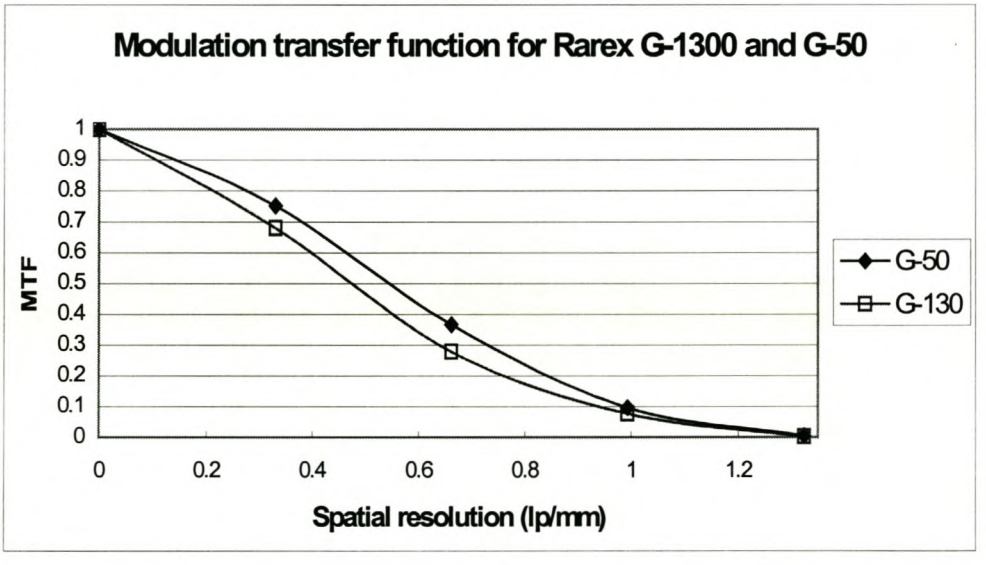

Figure 4-3: Modulation transfer functions for Rarex G-50, Rarex G-130, PFG and $CaWO_4$ obtained from the measured edge spread functions shown in Figure 4-2.

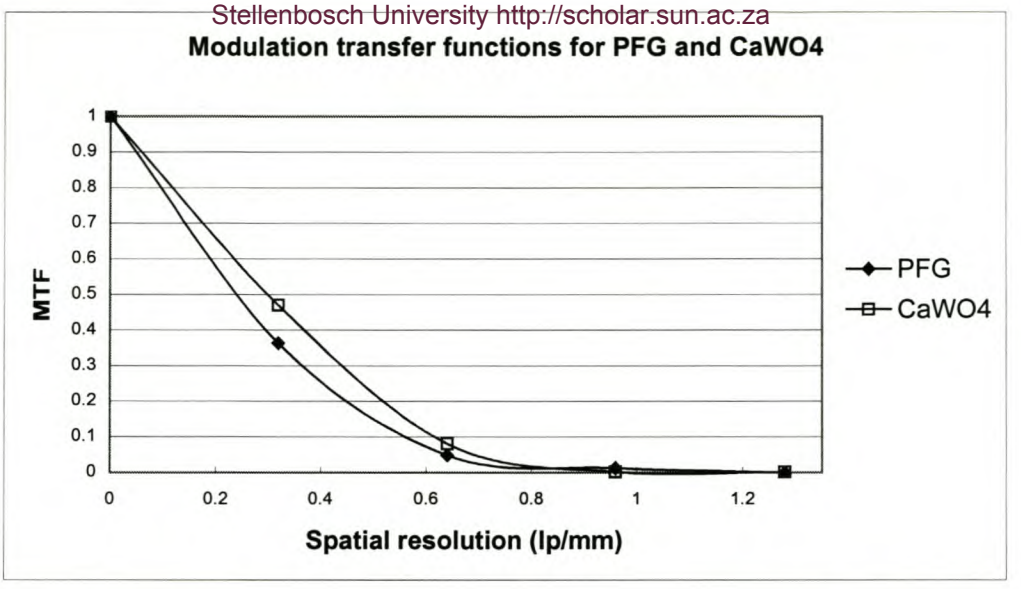

Figure 4-3: Modulation transfer functions for Rarex G-50, Rarex G-130, PFG and $CaWO_4$ obtained from the measured edge spread functions shown in Figure 4-2.

The gradients of the edge spread functions as well as the 2 % modulation value on the MTF graphs show that the same spatial resolution is measured for both the Rarex G-130 and G-50 screens. However, the obtainable screen resolution for Rarex G-50 is 6.3 lp/mm, while the screen resolution for Rarex G-130 screen is 5.0 lp/mm (see section 3.3.1). This shows that the CCD chip is responsible for the limitation in the maximum obtainable system resolution. The measured spatial resolution of the current set-up with field of view (FOV) of 290 x 190 mm^2 is 1.30 line pairs per millimetre and the Nyquist limit 1.32 lp/mm. For FOV of 160 x 110 mm^2 the measured resolution was 2.37 lp/mm with Nyquist limit 2.40 lp/mm. The fact that the system resolution measured with the Rarex G-130 screen is very close to the theoretical maximum obtainable resolution of the system (Nyquist frequency) confirms that the achieved resolution is limited by the CCD camera.

The measured resolution for the Rarex screens is considerably higher than for PFG and $CaWO_4$. For both PFG and $CaWO_4$, the system resolution is therefore not limited by the camera but by the screen resolution. Rarex G-130 screen produces a higher light yield than G-50 screen and is therefore chosen for the final set-up.

4.4 Image quality

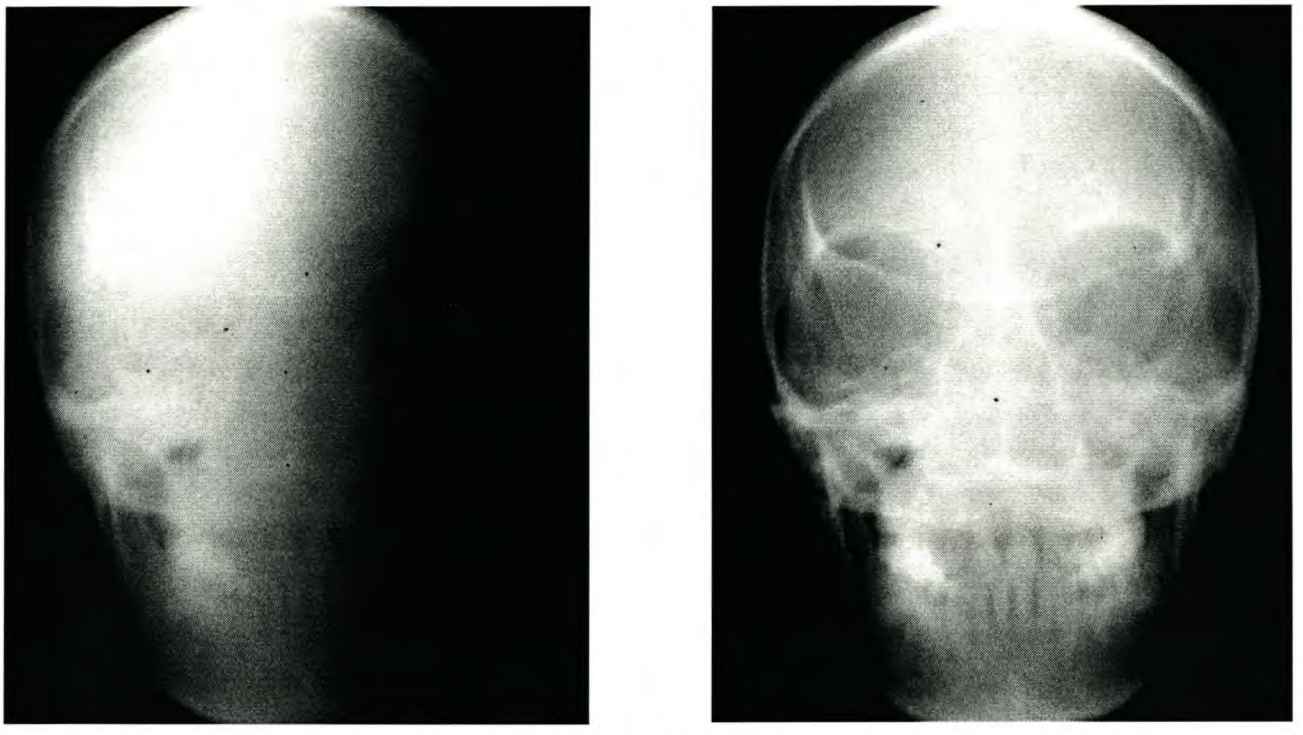

Figure 4-4: Digital AP images of a skull phantom indicating the effect of scattering between the scintillation screen and mirror. The first X-ray image (left) was taken with the screen and mirror placed in direct contact and the second image (right) with the mirror 70 mm away from the scintillation screen.

Light scattering between the mirror and the scintillator screen had a notable effect on the image quality. The AP images of a skull phantom used to investigate the scattering are shown in Figure 4-4. The first image (left) was taken with the mirror placed next to the screen. The second image (right) is obtained with 70 mm of the side of the mirror closest to the scintillator screen covered. The effect of the light scattering between the screen and mirror is clearly visible. This effect was also higher for small objects and large exposures.

The decrease in the image quality close to the edges due to the fish eye effect (see section 2.6.1, curvature of field) was lower in images obtained with using a 10 mm lens than for an 8 mm lens. A 10 mm lens is therefore used in the final set-up. Different set-up arrangements, for example the mirror angle were considered. The imaging system will be more compact and smaller if the angle between the screen and mirror is reduced, but the fish eye effect observed at the edges of the images was a-symmetrical.

Figures 4-5 and 4-6 shows a lateral X-ray image of the skull phantom obtained with the digital system compared with the image taken on radiographic film.

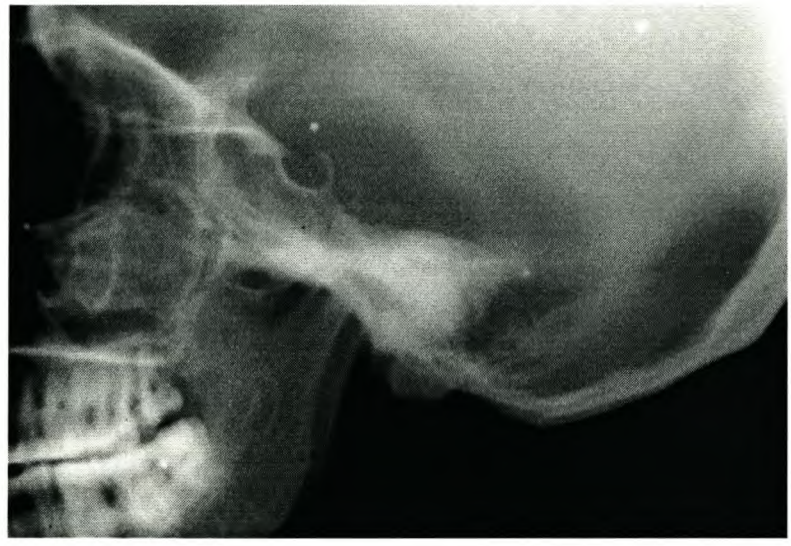

Figure 4-5: Digital radiographic X-ray image of a skull phantom (lateral view) taken with an exposure of 80 kVp and 20 mAs.

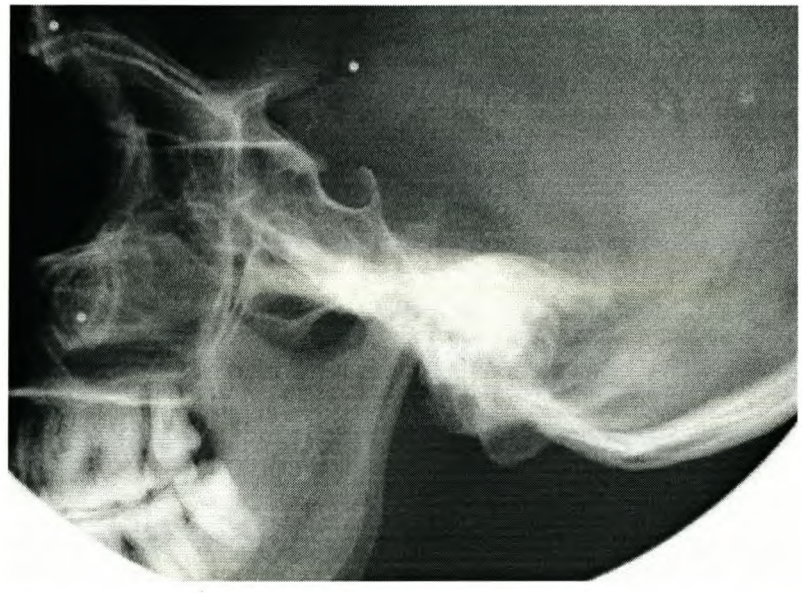

Figure 4-6: Lateral X-ray image of a skull phantom taken on film with an exposure of 80 kVp and 20 mAs.

The digital image has lower spatial resolution than an X-ray image taken on film, as expected. However, the image quality is sufficient for verification of the patient position, since the

important anatomical features are clearly visible. The digital X-ray image quality is also notably higher than that of the DRR (see Figure 1-5). The resolution of the DRR is limited by the slice thickness and spatial resolution of the CT scanner [Hou99].

4.5 Dose measurement

The absorbed dose at the screen entrance for different exposures is given in Table 4-2.

Table 4-2: Absorbed dose for different X-ray exposures measured at the source isocentre distance (SID) and converted to the source-screen distance (SFD).

Exposure	Exposure	Measurement	Dose at SID	Dose at SFD	Dose at SFD
kVp	mAs	nC	mR	mR	mGy
70	20	0.0154	68.7	34.8	0.35
80	10	0.013	58.0	29.4	0.29
80	15	0.0187	83.5	42.2	0.42
80	20	0.0228	102	51.5	0.52
85	20	0.0262	117	59.2	0.59
100	20	0.0385	172	87.0	0.87

An exposure of 80 kVp and 20 mAs is currently used for taking a lateral skull X-ray image on film. The quality of a digital X-ray image taken with 80 kVp and 15 mAs compared well with the image taken with 80kVp and 20 mAs (see Figure 4-7). Images taken with lower exposures (mAs values) appear grainy and have lower visible contrast between fine structures, as illustrated in Figure 4-7. However, the difference in image quality between the images obtained using 15 mAs and 20 mAs exposures is small and the lower exposure may therefore be used with the digital imaging system, resulting in a 19 % reduction in patient dose.

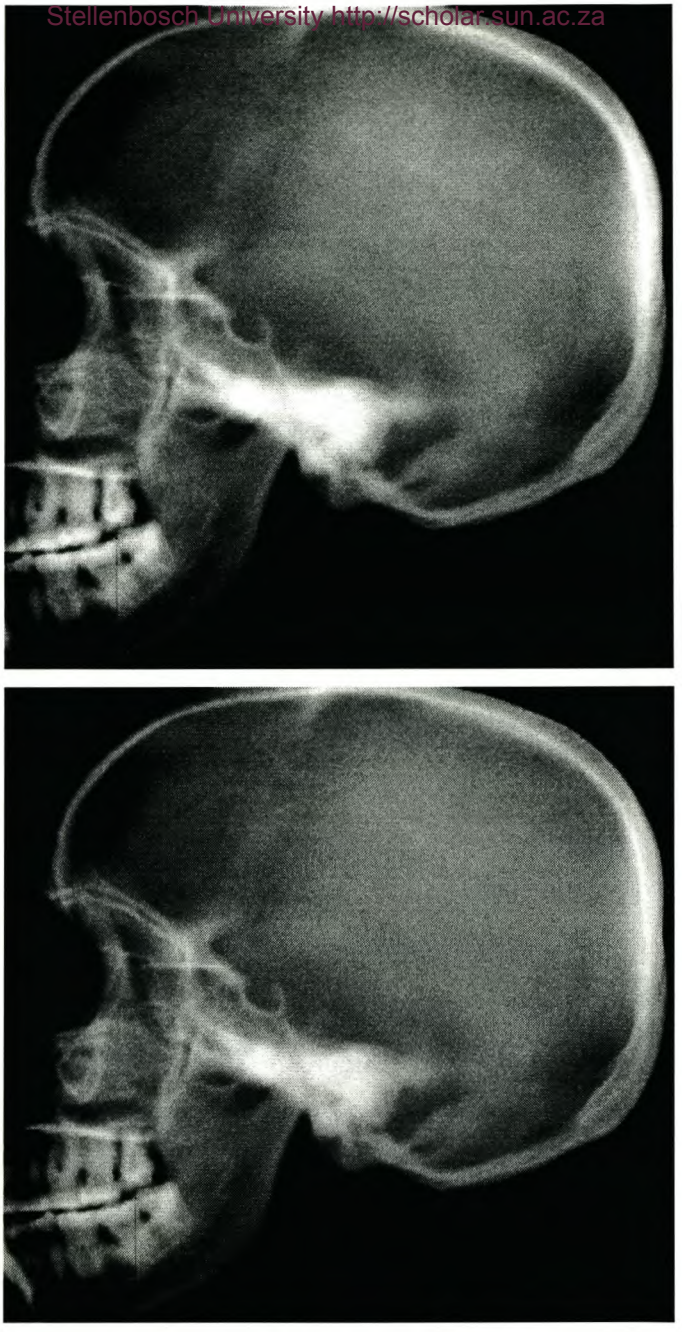

Figure 4-7: Comparison of the image quality of lateral digital images of the skull phantom taken with 15 mAs (top) and 20 mAs (bottom) with tube voltage 80 kVp.

Chapter 5

Conclusions

A simple digital X-ray imaging system has been developed successfully.

Rarex G-130, G-50 PFG and calcium tungstate scintillation screens were compared in terms of resolution and light yield. The resolution was measured with the modulation transfer function as well as with a test object. The MTF is a more accurate method for resolution measurement than the test object (wire phantom), especially for repeated measurements and for the comparison of the resolution obtained with the various screens. The same spatial resolution was measured with Rarex G-130 and G-50 (which has a higher screen resolution), showing that the scintillation screen does not limit the spatial resolution of the system. This is confirmed by the fact that the obtained (measured) resolution is equal to the Nyquist resolution limit set by the CCD chip resolution.

In screen-film systems the scintillation screen limits the resolution, since the screen is placed in direct contact with the film, which has considerably higher resolution than the screen. In a CCD camera based digital system, the system resolution is either limited by the optical scattering, camera resolution or the scintillation screen. The spatial resolution of the developed system is currently limited by the CCD chip resolution. The resolution can therefore be increased by increasing the CCD chip resolution, i.e. by using a CCD chip with more pixels of the same size (larger sensor size that maintains the same pixel density), or by decreasing the field of view. If the scintillation screen limits the system resolution, a screen with higher screen resolution, i.e. a thin screen or smaller grains should be used. The optical scattering may be minimised by using a high quality lens, a front silvered mirror and by increasing the distance between the mirror and the scintillation screen. The light yield is often compromised to reduce scatter of light between optical components by using larger set-up distances. The light tight cover of the system should also be lined with a high absorbing material to absorb the scattered light that reduces the image quality.

In most cases an increase in the resolution introduces a reduction in the light yield. This is confirmed by the fact that fast scintillation screens have lower resolution. This is also true for an

increase in the CCD chip resolution. If the camera resolution is doubled in both the vertical and horizontal directions i.e. if the number of pixels is doubled but the pixel size and all other parameters unchanged, the same amount of light will be projected onto four pixels instead of one. This means that the light yield per pixel will be reduced resulting in a lower signal to noise ratio. The reduction in light yield per pixel can be compensated for by reducing the screen-camera distance by half, but this will lead to an increase in the fish eye effect. The pixel size may also be reduced to obtain higher resolution, but at the expense of the light yield. The signal to noise ratio can also be increased by additional cooling of the CCD camera.

The light yield of the system is optimised by using a fast scintillation screen with high emission efficiency and good matching with the CCD chip sensitivity, a low atomic number screen mounting and a large aperture lens. The highest light yield was obtained with the Rarex G-130 screen due to its high emission efficiency and favourable matching with the Kodak KAF-0400 CCD chip. The Rarex G-130 screen is therefore used in the final set-up.

The spatial resolution and light yield are the primary limitations of the digital imaging system. The influence of the optical system on the spatial resolution can be improved by using a high quality lens to produce increased uniformity over the entire image and at the same time improve the light yield. High-resolution scintillation screens such as CsI:Tl screen are available for systems that require high resolution, but they are very expensive.

An important objective for any diagnostic imaging system is to reach the optimal balance between image quality and radiation dose. The patient dose and image quality are influenced by the radiation quality, the number of X-ray photons and the amount of scattered radiation. The quality of the digital images taken with a lower exposure (mAs) compared well with the film images and is sufficient for proton therapy positioning. The dose reduction achievable with the digital system (with the lower exposure) is 19 %.

A constraint of the digital system is the inability to focus the camera in real time. A method to focus the camera is presented in this thesis, but it is time consuming and should still be improved. The camera should also be firmly fixed after it has been focussed to ensure that the camera does not move with respect to the scintillation screen. The image sharpness and resolution should be verified regularly, as part of the quality assurance program. It is also

necessary to acquire a flat field image to correct for changes in the X-ray beam, which should also be included in the quality control program.

The digital system will reduce the patient set-up time considerably. An enormous amount of time will be saved on acquisition and furthermore the digital image can immediately be matched onto the DRR using computer software to verify the patient position. Additional improvements that have to be made before the digital system can be implemented include the synchronisation of the X-ray exposure with the capturing of the digital image and the development of a user-friendly software interface that may be used by the radiographers.

Appendix A

A.1 Sampling Theorem

If F_{max} is the highest frequency component in an analog signal $x_a(t)$ and the signal is sampled at a rate $Fs > 2F_{max}$, then $x_a(t)$ can be exactly recovered from its sample values using the interpolation function

$$x_a(t) = \sum_{n=-\infty}^{\infty} x_a\left(\frac{n}{2B}\right)\frac{\sin 2\pi B(t - n/2B)}{2\pi B(t - n/2B)} \tag{A-1}$$

[Pro96].

A.2 Quantisation of sinusoidal signals and signal to quantisation noise ratio

The signal to quantisation noise ratio can be expressed as the ratio of the signal power to the noise power [Pro96].

The signal power (average) for a sinusoidal signal is given by

$$P_i = \frac{1}{T_p}\int_0^{T_p}(A\cos\Omega_0 t)^2\,dt = \frac{A^2}{2}, \tag{A-2}$$

where A is the signal amplitude which will extend over the range of the analog-to-digital converter $(2A)$ for the largest sinusoidal signal.

If the range of the analog-to-digital converter is $2A$, the quantisation step size Δ is given by

$$\Delta = \frac{2A}{2^b} \tag{A-3}$$

where b is the number of available bits after conversion.

The mean-square error power is given by:

$$P_q = \frac{1}{2\tau}\int_{-\tau}^{\tau} e_q^2(t)dt = \frac{1}{\tau}\int_0^{\tau} e_q^2(t)dt \tag{A-3}$$

The quantisation error e_q is limited to the quantisation step interval:

$$-\frac{\Delta}{2\tau} \leq e_q(t) \leq \frac{\Delta}{2\tau};\ \tau < t < \tau. \tag{A-4}$$

The quantisation error power then becomes

$$P_q = \frac{1}{\tau}\int_0^{\tau}\left(\frac{\Delta}{2\tau}\right)^2 t^2 dt = \frac{\Delta^2}{12}. \tag{A-5}$$

Substituting equation A-3 into A-5, the quantisation error power is given by:

$$P_q = \frac{A^2/3}{2^{2b}} \tag{A-6}$$

The signal-to-quantisation noise ratio, $\text{SQNR} = \dfrac{\text{Signal power}}{\text{Noise power}}$, is given by:

$$\text{SQNR} = \frac{P_i}{P_q} = \frac{3}{2}2^{2b} \tag{A-7}$$

or, expressed in decibels

$$\text{SQNR(dB)} = 10\log_{10}\text{SQNR} = 1.76 + 6.02b \tag{A-8}$$

A.3 Picture of box used for experiments

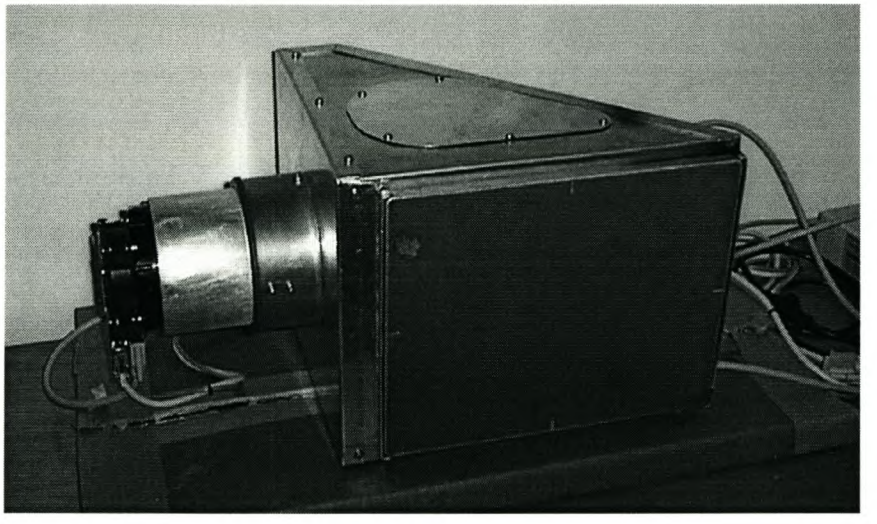

A.4 Drawing of final box

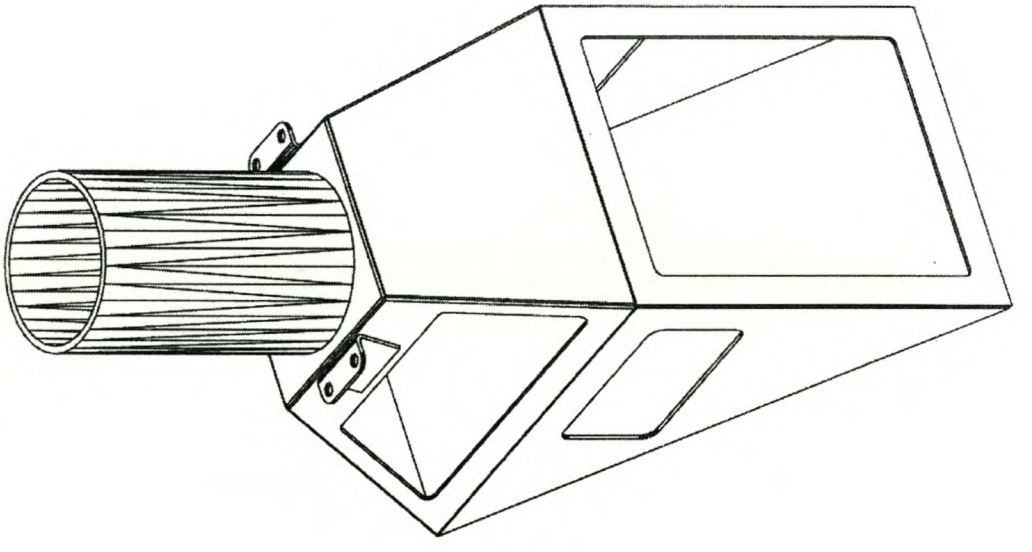

References

[ACR93] ACR-NEMA Digital Imaging and Communications Standards Committee formed by the American College of Radiology (ACR) and the National Electrical Manufacturers' Association (NEMA) in 1982. NEMA Standards Publication PS3, 1993. http://www.leadtools.com/home2/DICOM/DICOMstnd.htm

[Aki96] Akine Y. Introduction to proton therapy. Institute of Clinical Medicine, Univeristy of Tsukuba http://www-medical.kek.jp/Intro2.html, 1996.

[Alt96] Althof V G M, De Boer J C J, Huizenga H, Stroom J C, Visser A G and Swanenburg B N. Physical characteristics of a commercial electronic portal imaging device. Med. Phys. 23(11), 1845-1855, 1996.

[App99] Applied Scintillation Technologies Ltd. http://www.appscintech.com, 1999.

[Att86] Attix F H. Introduction to Radiological Physics and radiation Dosimetry. John Wiley & Sons, 1986.

[Bar98] Barkhof J. Performance of the CCD camera for dosimetry applications. M.Sc. Thesis, Rijksuniversiteit, Groningen, the Netherlands, 1998.

[Bar81] Barret H H and Swindell W. Radiological Imaging – The Theory of Image Formation, Detection, and Processing. Volume 1. Academic Press 111 Fifth Avenue, New York, 10003 (A subsidiary of Harcourt Brace Jovanovich, Publishers), 1981.

[Bic99] Bicron Business Unit of Saint-Gobain Industrial Ceramics, Inc. http://www.bicron.com, 1999.

[Bo98a] Boon S N. Dosimetry and quality control of scanning proton beams. Ponsen & Looijen BV, Wageningen, the Netherlands. Ph. D Thesis, Rijksuniversiteit, Groningen, 1998.

[Bo98b] Boon S N, Van Luijk P, Schippers J M, Meertens H, Denis J M, Vynckier S, Medin J and Grusell E. Fast 2D phantom dosimetry for scanning proton beams. Med. Phys. 25(4), 464-475, 1998.

[Boy92] Boyer A L, Antonuk L, Fenster A, Van Herk M, Meertens H, Munro P, Reinstein L E and Wong J. A review of electronic portal imaging devices (EPIDs). Med. Phys. 19 (1), 1-16, 1992.

[Bra98] Brandeis University Detector Group. CCD-based Detector for Full-field Digital Mammography. http://www.rose.brandeis.edu/users/mammo/fullfield.html#A, 1998.

[Bri88] Brigham E O. The Fast Fourier Transform and its applications. Prentice-Hall, Englewood Cliffs, New Jersey, 1988.

[Cou81] Coulam C M, Erickson J J, Rollo F D and James A E. The physical basis of medical imaging. Prentice-Hall, Inc., Appleton-Century-Crofts, New York, 1981.

[Cur90] Curry T S, Dowdey J E and Murry R C. Christensen's Physics of Diagnostic Radiology. Lea & Febiger, Philadelphia, London, Fourth Edition, 1990.

[Dro85] Droege R T and Rzeszotarski M S. An MTF method immune to aliasing. Med. Phys. 12 (6), 721-725, 1985.

[Edm97] Edmund scientific – Industrial Optics Division: Optics and Optical Instruments Catalog, 1997.

[Fah95] Fahrig R, Rowlands J A and Yaffe, J J. X-ray imaging with amorphous selenium: Detective quantum efficiency of photoconductive receptors for digital mammography. Med. Phys. 22, 153-160, 1995.

[Fis81] Fisher M G. Objective physical measurements: Physical Aspects of Medical Imaging. Moores B M, Parker R P and Pullan B R. John Wiley & Sons Ltd, 1981.

[Fuj85] Fujita H, Doi K and Giger M L. Investigation of basic imaging properties in digital radiography. 6. MTFs of II-TV digital imaging systems. Med. Phys 12 (6), 713-720, 1985.

[Fuj89] Fujita H, Ueda K, Morishita J, Fujikawa T, Ohtsuka A and Sai T. Basic imaging properties of a computed radiographic system with photostimulable phosphors. Med. Phys. 16 (1), 52-59, 1989.

[Fuj92] Fujita H, Tsai D, Itoh T, Doi K, Morishita J, Ueda K and Ohtsuka A. A simple method for determining the modulation transfer function in digital radiography. IEEE Transactions on medical imaging, Vol. 11 No. 1, 34-39, 1992.

[Gia85] Giakoumakis G E and Miliotis D M. Light angular distribution of fluorescent screens excited by x-rays. Phys. Med. Biol., Vol 30, (1), 21-29, 1985.

[Gi84a] Geiger M L and Doi K. Investigation of basic imaging properties in digital radiography. Vol. 1. Modulation transfer function. Med. Phys. 11 (3), 287-295, 1984.

[Gi84b] Geiger M L, Doi K and Metz C E. Investigation of basic imaging properties in digital radiography. Vol. 2. Noise Wiener spectrum. Med. Phys. 11 (6), 797-805, 1984.

[Gon93] Gonzalez R C and Woods R E. Digital Image Processing. Addison-Wesley Publishing company, Inc., 1993.

[Ham99] Hamamatsu Photonics UK Ltd. http://www.hamamatsu.com, 1999.

[Hal93] Halliday D, Resnick R and Walker J. Fundamentals of Physics. Fourth edition, John Wiley & Sons, 1993.

[Har88] Harrison R M. Digital radiography (Review article). Phys. Med. Biol. Vol. 33 No 7, 751-784, 1988.

[Hou99] Hough J K. Assessment of and Improvements to a Stereophotogrammetric Patient Positioning System for Proton Therapy. M.Phil. Thesis – University of Cape Town, 1999.

[Ind99] http://www.industrialtechnology.co.uk/1999/jan/siraimaging.html.

[Jon95] Jones D T L. The Only Proton Therapy Facility in the Southern Hemisphere. Ion Beams in Tumor Therapy edited by Linz U. Weinheim, Germany: Chapman & Hall GmbH, 350 – 359, 1995.

[Joh83] Johns H E and Cunningham J R. The physics of radiology. Fourth edition. Charles C Thomas publisher, 1983.

[Kno89] Knoll G F. Radiation Detection and Measurement. John Wiley & Sons, Second edition, 1989.

[Koc94] Koch A. Nuclear Instruments and Methods in Physics Research A 348, 654-658, 1994.

[Kod92] Documentation of Kodak KAF-0400 CCD chip. Eastman Kodak Company – Microelectronics Technology Division, Rochester NY. http://www.kodak.co.za, 1992.

[Lam99] Lambert Instruments – CCD camera specifications. Leutingewolde, The Netherlands. Lambert-instruments.com.

[Liu94] Liu H, Karellas A, Harris L and D'Orsi C J. Methods to calculate the lens efficiency in optically coupled CCD X-ray imaging systems. Med. Phys 21 (7), 1193 –1195, 1994.

[Mar99] Martin C J, Sutton D G and Sharp P F. Balancing patient dose and image quality. Applied Radiation and Isotopes (50), 1-19, 1999.

[Mci99] MCI Optonix – Division of USR Optonix, Cedar Knolls, NJ. http://www.mcio.com, 1999.

[Mer79] Meredith W J and Massey J B. Fundamental Physics of Radiology. Bristol: John Wright & Sons, Third edition 1979.

[Mo81] Moores B M, Parker RP and Pullan B R. Physical Aspects of Medical Imaging - Proceedings of a meeting held at the University of Manchester, 25th – 27th June, 1980. John Wiley & Sons, 1981.

[Mu90a] Munro P, Rawlinson J A and Fenster A. A digital fluoroscopic imaging device for radiotherapy localisation. Int. J. Radiat. Oncol. Biol. Phys. 18, 641-649, 1990.

[Mu90b] Munro P, Rawlinson J A and Fenster A. Therapy imaging: A signal-to-noise analysis of a fluoroscopic imaging system for radiotherapy localisation. Med. Phys. 17(5), 763-772, 1990.

[Nei94] Neitzel U, Maack I and Gunther-Kohfahl S. Image quality of a digital chest radiography system based on a selenium detector. Med. Phys. 21(4), 509-516, 1994.

[Pro96] Proakis J G and Manolakis D G. Digital signal processing – Principles, Algorithms, and applications. Third edition, Prentice Hall International Editions, 1996.

[Ryn95] Ryneveld S C. Measurement of proton beam dose profiles using a sensitive scintillation screen observed with a CCD camera. M.Sc. Thesis – University of British Columbia, 1995.

[Sit00] An Introduction to Scientific Imaging Charge-Coupled Devices. SITe CCD technology. http://www.site-inc.com/pdf/introdat.pdf, 2000.

[Spr93] Sprawls P JR. Physical Principles of Medical Imaging. Aspen Publishers, Gaithersburg, Md, Second edition – Medical Physics Publishing, 1996.

[Thw96] Thwaites J H, Rafferty M W, Gray N, Black J and Stock B. A patient dose survey for femoral arteriogram diagnostic radiographic examinations using a dose-area product meter. Phys. Med. Biol. 41, 899-904, 1996.

[Yut97] Yu T and Bone J M. Lens coupling efficiency: Derivation and application under differing geometrical assumptions. Med. Phys 24 (4), 565 –570, 1997.